

# **CHARACTERISATION OF A MAX-DOAS INSTRUMENT AND APPLICATION TO SATELLITE VALIDATION**

By  
David Cudjoe ADUKPO  
B.Sc. , MPhil. (Physics)

SUBMITTED TO  
THE BOARD OF POSTGRADUATE PROGRAMME IN ENVIRONMENTAL PHYSICS,  
INSTITUTE OF ENVIRONMENTAL PHYSICS AND REMOTE SENSING, UNIVERSITY OF BREMEN  
FOR THE AWARD OF MSc. IN ENVIRONMENTAL PHYSICS.

September, 2002

## DECLARATION

I herewith declare that I did the written work on my own and only with the means as indicated.

.....  
David Cudjoe ADUKPO  
(Candidate)

.....  
Date

.....  
Prof. Dr. J. P. BURROWS  
(Supervisor & First Reviewer)

.....  
Date

.....  
Prof. Dr. J. BLECK-NEUHAUS  
(Second Reviewer)

.....  
Date

.....  
Dr. Andreas RICHTER  
(Thesis Tutor)

.....  
Date

## DEDICATION

This work is dedicated to my lovely wife, Frau Genevieve Etornam ADUKPO, for her support, warmth, toil and sacrifice during the preparation of this thesis.

**“ I will praise you, O Lord, with all my heart; I will tell of all your wonders. I will be glad and rejoice in you; . . . . (Psalm 9: 1 & 2) ”**

## Abstract

Starting from 1993, two zenith sky DOAS instruments have been operated on the roof of the Institute of Environmental Physics, University of Bremen (IUP-Bremen), 53 °N to continuously monitor column amounts of absorbers like Ozone and Nitrogen Dioxide. New innovations have been made to the standard setup over the years. Details of the Multi-Axis DOAS (MAX-DOAS) instrumentation, involving the use of different lines of sight near the horizon as additional sources of light are presented. Results of the first calibration measurements from one of the new instruments are outlined with a revelation of a low saturation level of 16 to 26 kilocounts of the Charged Coupled Device (CCD) from the manufacturers. The instrument slit function was noted to be asymmetric and recommendations were made for further adjustment. Measurements over Bremen and Nairobi for July 27, August 1 and 24, 2002 using the MAX-DOAS instruments show a lot of tropospheric and stratospheric NO<sub>2</sub> over Nairobi and Bremen respectively. About  $1.4 \times 10^{17}$  molec / cm<sup>2</sup> was measured over Nairobi around the boundary layer (Off-axis 4 °). Of particular interest is the heavy vehicular pollution detected in the early hours of August 24 in Nairobi. The qualitative result presented is an indication that the new technique derives not only the column amounts of the trace gases but also is capable of providing information about the location of the absorbers. Finally, 2001 total Ozone columns measured over Bremen using the zenith sky DOAS were validated against the TOMS and GOME satellite instruments. The result showed nearly the same scatter (RMS value of ~13 Dobson Units) difference among the three instruments for the summer months of July to September. Large variability was noticed during the winter-spring season and this was primarily due to the large pixel size of the satellite instruments.

# Table of Content

<b>Abstract.....</b>	<b>iv</b>
<b>1 Introduction.....</b>	<b>1</b>
<b>2 Chemistry of the Atmosphere.....</b>	<b>6</b>
2.1 Stratospheric Chemistry	6
2.1.1 NOX – catalytic cycle	9
2.2 Tropospheric Chemistry	12
2.2.1 Tropospheric Ozone production	13
2.2.2 Photochemical air Pollution; Summer Smog	14
<b>3 DOAS Measurement Techniques .....</b>	<b>16</b>
3.1 The Dobson’s Equation	17
3.2 Differential Cross-sections	18
3.3 Off-Axis against Zenith-Sky Measurements	20
<b>4 Instruments and Techniques of Measurements.....</b>	<b>24</b>
4.1 Instrumental Design	24
4.1.1 Spectrometer	25
4.1.2 The CCD	27
4.1.3 The Telescope	30
4.2 The MAX-DOAS Instrument	32
4.2.1 Mode of operation of the MAX-DOAS	34
<b>5 Calibration Measurements.....</b>	<b>37</b>
5.1 Dark Measurements	38
5.1.1 Explanations	43
5.2 Linearity Measurements	44

5.3	Polarisation Dependency Measurement	46
5.4	Slit function Measurement	48
5.5	Summary	50
<b>6</b>	<b>Data.....</b>	<b>51</b>
6.1	GOME	51
6.2	EARTH PROBE TOMS	53
6.3	DOAS BREMEN	55
6.4	Results and Discussion	56
6.5	MAX-DOAS Measurement over Bremen and Nairobi	59
6.5.1	First Off-Axis Measurement in the Tropics (Nairobi)	59
6.2.1	Bremen Off – Axis Measurement	62
<b>7</b>	<b>Summary and Conclusion.....</b>	<b>64</b>
	<b>References.....</b>	<b>68</b>
	<b>Acknowledgement.....</b>	<b>72</b>

# 1 Introduction

In the 1980s the ozone hole was found above the Antarctic continent and this phenomenon became a big scientific and political issue. Due to anthropogenic halogen compounds and strong polar vortex during winter, severe ozone depletion was measured. The theory is quite complicated but could be simplified as: the hole forms over the Antarctica because it is really cold (about  $-78$  to  $-86$  °C) there during polar winters. That is during the polar winters, despite the dryness of the stratosphere, the temperature drops low enough for condensation to occur. The Polar Stratospheric Clouds (PSCs) are important components of the ozone depletion process in the polar regions of Antarctica and the Arctic. The PSCs provide the surfaces upon which chemical reactions involved in ozone destruction take place. The clouds are made of a mixture of water ice crystals, crystals of water ice mixed with nitric acid, as well as droplets of liquid water mixed with nitric acid and sulphuric acid. In other parts of the world the stratosphere is too warm for these clouds to form, which is one reason why the 'ozone hole' is confined to the Antarctic region. The temptation to think that because the worst ozone depletion happens at the South Pole and that the rest of the world is safe is far from the point. Ozone depletion still happens all over the world. Though much lesser in extent than the Antarctic ozone loss, global ozone loss can have harmful effects on all forms of life, including humans.

In the last years, the role of anthropogenic emissions on the global tropospheric ozone budget has been the focus of intense scientific research. The improvement of our understanding of and the assessment of the impact of the interaction between mankind's activities and the earth's environment is one of the most important challenges facing our generation. In the tropical regions biomass burning seems to play an important role in the tropospheric ozone formation. In addition to direct production in the regions of fires (for instance in Southern

Africa, Brazil and Indonesia), the emission of ozone precursors from the fires and subsequent transport to remote regions including the Southern Atlantic has been recognised to be an important process. Consequently, the emissions released as a result of anthropogenic activities are altering the global composition of trace atmospheric constituents. Anthropogenically induced climate change may be more significant than the changes experienced by the biosphere during the last 10,000 years. Pollution resulting from the combustion of hydrocarbons and pyrogenic (biomass burning) emissions, and the ozone hole are two quick examples which require reliable scientific findings at the global scale to assist in the development of regional, national and international policy.

The challenge posed by the above scenario saw a development in recent years of different measurement techniques and tools (in-situ and remote sensing measurements) to determining the long-term changes in atmospheric constituent concentrations. This involves measurements made from the ground, aircraft, balloons, and satellites. Measurements from ground-based UV / visible spectrometers have provided an abundance of information about the chemistry of the atmosphere in the recent past, particularly Antarctic ozone chemistry (Solomon et al., 1987b; Sanders et al., 1989; Mount et al., 1987). Traditionally ground-based measurements employing a zenith-sky viewing geometry have been made for measuring stratospheric constituents such as ozone and nitrogen dioxide (NO<sub>2</sub>) by means of differential optical absorption spectroscopy (DOAS). More recently, DOAS has been successfully applied to nadir-viewing instruments on aircraft (McElroy et al., 1999) and satellite (Burrows et al., 1999) platforms.

DOAS is a technique of remote sensing allowing the determination of the abundance of atmospheric trace species by use of their structured absorption bands in the UV and visible spectral regions. It is one of the most widely applied spectroscopic methods in atmospheric

research. Its technique is based on the difference in absorption at different wavelengths. With the DOAS method, trace species are identified using the structures in their UV / visible absorption cross-sections. As a result only those species which show significant and structured absorption in the UV / visible wavelength range can be observed. Relevant molecules include  $\text{NO}_2$ ,  $\text{O}_3$ ,  $\text{BrO}$ ,  $\text{OCIO}$ ,  $\text{IO}$ , ... ,  $\text{HCHO}$ ,  $\text{H}_2\text{O}$ ,  $\text{O}_4$ , or  $\text{SO}_2$ . The structures are used to distinguish between different absorber and also between absorption by trace gases and scattering by air molecules and aerosols. For instance, the atmospheric  $\text{O}_3$  shows a structured absorption in the Huggins bands.

Measurements from the Global Ozone Monitoring Experiment (GOME) have been analysed for tropospheric  $\text{NO}_2$  using the DOAS method. A case study of tropospheric  $\text{NO}_2$  above Africa in fall 1997 showed the influence of both biomass burning and lightning. Results from that study revealed that substantial amounts of  $\text{NO}_2$  are present in the free troposphere over the African continent and in the regions over the Southern Atlantic and the Indian Ocean (Richter et al, 2001).

The  $\text{NO}_2$  radical is one of the key species in both stratospheric and tropospheric chemistry. In the stratosphere, it is involved in ozone destruction and the conversion of active halogen oxides into less active reservoirs. In the troposphere, it is one of the most important ozone precursors and locally also contributes to radiative forcing. The main tropospheric sources of  $\text{NO}_x$  (family of nitrogen oxides,  $\text{NO}+\text{NO}_2$ ) are soil emissions, industrial burning processes, biomass burning and lightning, adding up to an estimated total of 38 TgN per year (Lamarque et al 1996). While the main sources and source regions of  $\text{NO}_x$  are known, large uncertainties remain on the individual source strengths and their latitudinal and seasonal variation. With the new generation of nadir viewing UV / visible satellite instruments measuring at moderate spectral resolution such as GOME, measurements of tropospheric  $\text{NO}_2$  from space have

become possible, and a clearer picture of the global NO<sub>2</sub> concentration is evolving. Currently, these measurements are still of limited accuracy, but ongoing developments (SCIAMACHY-Scanning Imaging Absorption spectroMeter of Atmospheric CHartographY on ENVISAT) and the retrieval techniques will improve the accuracy of the satellite data to a point where they cannot only be used in a qualitative, but also in a quantitative sense (Burrows et al, 1999).

Experience from GOME validation showed that DOAS UV / visible instruments can provide long-term validation, that tropical stations are mandatory and that tropospheric products need extra validation (Burrows et al, 1999). To fill the gap at low latitudes, BREDOM (Bremen DOAS Measurement Network) was proposed consisting of seven ground-based DOAS stations with three of them at tropical sites (Nairobi, Merida and Kaashidoo) and two at polar sites (Ny Alesund and Summit) in addition to two stations at mid-latitudes (Bremen and Zugspitze). The extension on the existing DOAS network will enhance the capability to monitor the troposphere. The DOAS network in effect would help in facilitating the realisation of the mission concept of SCIAMACHY. Some of the set goals for SCIAMACHY include the detection of constituents relevant for observation of global atmospheric change such as stratospheric ozone depletion as well as global warming and tropospheric pollution. The multi-axis viewing DOAS planned for BREDOM will foster the distinction between stratospheric and tropospheric compounds for the validation of SCIAMACHY products as well as for local research. In view of the foregoing, this work is intended to use the new generation Multiple AXis - DOAS (MAX-DOAS) instrument of the Institute of Environmental Physics (IUP), Bremen to measure the tropospheric O<sub>3</sub> and NO<sub>2</sub> in the tropics (Nairobi). This is well suited because of the multiple-viewing directions incorporated into the instrument, a new innovation. The results will be used for the validation of the SCIAMACHY instrument on board the ENVISAT satellite. The comparison of the ground based and satellite

data is also well suited to derive unique information about several atmospheric processes, which are currently under intense scientific debate, among which are;

- Investigation of the suggested tropospheric ‘background’ BrO concentration
- -Quantification of the tropospheric NO<sub>2</sub> budget
- -Quantification of the oxidation capacity of the atmosphere.

In order to achieve these objectives both off-axis and zenith-sky measurements from the multi-axis scattered light DOAS instruments from the ground and from aircraft, probing the troposphere using passive DOAS, is critical. The Off-Axis measurements will have sensitivity towards the troposphere whilst the zenith-sky viewing direction will reveal much of the stratospheric absorbers.

In this work, results of the characterisation of the new instrument are presented. In addition, analysis of the O<sub>3</sub> and NO<sub>2</sub> data from the Bremen instrument is also considered. The work is structured in the following way: in the first chapter the general introduction is given – contemporary scientific questions. This is followed by a short overview on the stratospheric and tropospheric O<sub>3</sub> and NO<sub>2</sub> chemistry in the third chapter. The background to DOAS, and the DOAS principle and distinction between the off-axis and the zenith sky measurements are discussed in chapter three. The fourth chapter introduces the instrumentation of the MAX-DOAS and its main features followed by results from the characterisation of the new instrument in chapter five. Next is the comparison of the ground-based measurements with GOME and TOMS and the very first results from Nairobi measurements. Lastly the main results are summarised and possible conclusion given in the seventh chapter. Recommendations are also made for possible future investigations.

## 2 Chemistry of the Atmosphere

Mankind's understanding of the chemistry of our atmosphere is based on early work studies of air pollution; these are often treated in the context of an overall system. This approach starts with the various sources of anthropogenic and natural emissions and tracks the resulting pollutants through their atmospheric transport, transformations, and ambient concentrations – on local, regional, and global scales – to their ultimate chemical and physical fates, including their impacts on our health and environment. Thus the chemistry of the atmosphere encompasses the chemistry of the globe, from polluted to 'clean', remote regions and from the region closest to the earth's surface, the troposphere ( $\leq 10\text{-}15$  km), through the tropopause ( $\sim 10\text{-}15$  km) into the upper atmosphere – which, for the purpose of this work, is limited to the stratosphere ( $\sim 10\text{-}50$  km). Chemical and physical processes occurring at the earth's surface can impact the stratosphere and vice versa. Though some early studies perceived the tropopause as being a 'barrier' between the lower and upper atmospheres, it has become increasingly clear that the troposphere and the stratosphere are intimately connected. In this chapter the ozone and  $\text{NO}_2$  chemistry in the stratosphere and the troposphere are briefly introduced.

### 2.1 Stratospheric Chemistry

Ozone is the most important trace constituent in the stratosphere. Discovered in the 19<sup>th</sup> century, its importance as an atmospheric gas became apparent in the early part of the 20<sup>th</sup> century when the first quantitative measurements of the ozone column were carried out in Europe. The stratospheric ozone layer, centred at about 20 km above the surface of the Earth (Figure 2.1), protects life on Earth by the absorption of the UV radiation from the Sun.

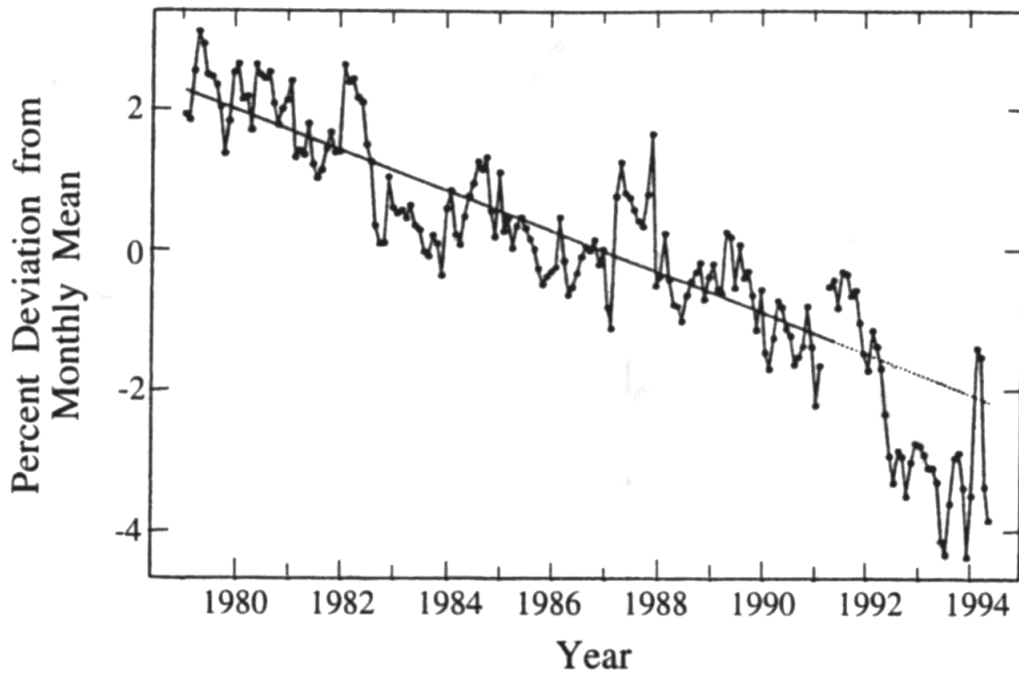


**Figure 2.1** The natural ozone layer: vertical and latitudinal distribution of the ozone number density ( $10^{12}$  molecules  $\text{cm}^{-3}$ ) at the equinox, based on measurements taken in the 1960s. *From Wayne, R.P., Chemistry of Atmospheres, Oxford, 1991.*

It is observed that the ozone mixing ratio is lowest in the tropics and that the height of the ozone maximum decreases with latitude. Ozone is mostly produced at the equator and transported to mid-latitudes and finally subsides in the Polar Regions.

Figure 2.2 shows total ozone column (area-weighted between  $60^\circ$  S and  $60^\circ$  N) from the NOAA-11 satellite using a solar backscattered ultraviolet spectrometer for the period, January 1979 to May 1994. Measurements of the vertical profile of the change in ozone concentration have established that decreases are focused in the lower stratosphere in the regions of highest ozone concentration.

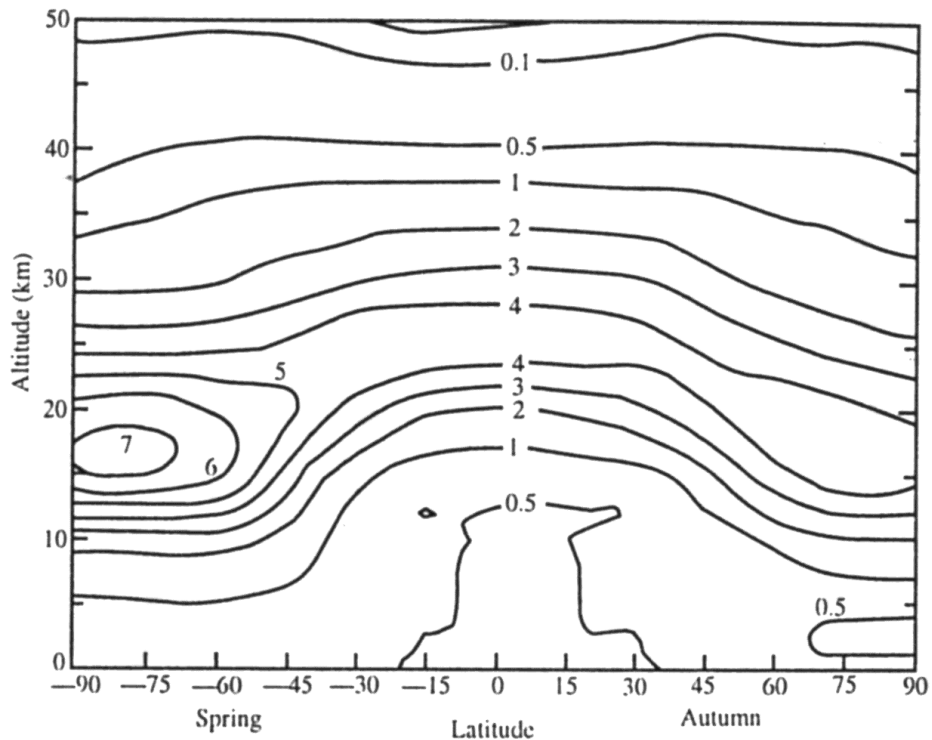


**Figure 2.2** Total ozone column (60 °N to 60 °S) from January 1979 to May 1994 measured by the solar backscattered ultraviolet spectrometer, SBUV (World Meteorological Organisation, 1994). The solid line is a least squares fit to the data through May 1991. The dashed line is an extrapolation through May 1994. The annual cycle and the quasi-biennial oscillation (QBO) have been removed. *From: Seinfeld and Pandis, Atmospheric Chemistry and Physics, John Wiley & Sons, 1998*

This led to a lot of open questions, of great scientific interest, related to the chemistry of the stratosphere:

- what are the production and loss mechanisms for the stratospheric ozone?
- what is the effect of anthropogenic emissions on stratospheric ozone, both past and future
- what are the mechanisms responsible for the spectacular ozone decreases in the Antarctic ozone hole
- does the aerosol layer play any role in the gas-phase chemistry of the stratosphere
- what is the source of the stratospheric aerosol layer
- what effect on stratospheric ozone would result from a fleet of supersonic aircraft.

In this section only the production and loss mechanism is highlighted with nitrogen oxide as a major player. This is also representative of the basic idea underpinning the DOAS innovation (the Multi- Axis DOAS technique) that has photochemical smog production and pollution in urban areas detection as a priority. Today in many major urban areas, the primary pollutants are NO<sub>x</sub> (mainly NO) and volatile organic compounds (VOC), which undergo photochemical reactions in sunlight to form a host of secondary pollutants, the most prominent of which is ozone.

Chapman (1930) proposed that the ozone layer originates from the photolysis of atmospheric O<sub>2</sub>. The bond energy of the O<sub>2</sub> molecule (498 kJ mol<sup>-1</sup>) corresponds to the energy of a 240 nm UV photon; only photons of wavelengths less than 240 nm can photolyse the O<sub>2</sub> molecule:



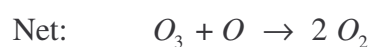
The O atoms (2.1a) are in the ground-level triplet state and are highly reactive due to their two unpaired electrons. The O atom (2.1c) is in an excited singlet state and is rapidly stabilised by collision with N<sub>2</sub> or O<sub>2</sub>. It is noted that reaction 2.1c is not a terminal sink for O<sub>3</sub> since the O atom product may recombine with O<sub>2</sub> by 2.1b to regenerate O<sub>3</sub>. This leads to a rapid cycling between O and O<sub>3</sub> (Chapman cycle).

### 2.1.1 NO<sub>x</sub> – catalytic cycle

A major breakthrough in understanding the stratospheric ozone came about as a result of discussion of the implementation of a large fleet of supersonic aircrafts flying in the stratosphere. This led to the discovery that NO can effectively destroy ozone. The principal

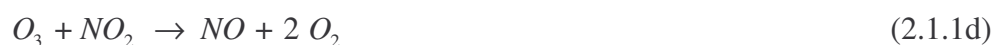
natural source of  $\text{NO}_x$  ( $\text{NO}$  and  $\text{NO}_2$ ) in the stratosphere is the transport of  $\text{N}_2\text{O}$  from the troposphere and subsequent reaction with singlet O atom or emission from aircraft.

Nitrogen oxides react with ozone in two reaction mechanisms:

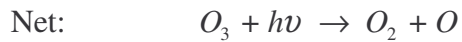


This cycling between  $\text{NO}$  and  $\text{NO}_2$  takes place on a time scale of about one minute during daytime. At night production of atomic oxygen ceases so reaction 2.1.1b is the daytime partitioning between  $\text{NO}$  and  $\text{NO}_2$  that is being controlled by atomic oxygen (O).

In the lower stratosphere where ozone is more prevalent, the second mechanism of the  $\text{NO}_x$  cycle is that one which leads to an overall loss of odd oxygen (net of reaction 2.1.1c and 2.1.1d).



Each cycle consumes two O<sub>3</sub> molecules. In addition to these there is the null cycle:



It has no net effect on O<sub>3</sub> and is called a null cycle. It causes, however, rapid exchange between NO and NO<sub>2</sub>. The NO<sub>2</sub> has the option of either photolysing (null cycle) or reacting with O or O<sub>3</sub> (O<sub>3</sub> loss cycle).

Similar cycles exist for HO<sub>x</sub>, ClO<sub>x</sub> and BrO<sub>x</sub>. Ozone depletion by NO<sub>x</sub> catalysis occurs at higher altitudes while interference with HO<sub>x</sub>, ClO<sub>x</sub> and BrO<sub>x</sub> rather takes place at lower altitudes. By using HO<sub>x</sub> and NO<sub>x</sub> cycles together (HO<sub>x</sub> / NO<sub>x</sub> coupling) with the Chapman mechanism, models can accurately simulate stratospheric ozone (Noble Prize 1995 for Paul Crutzen).

However, human emissions change the concentrations of atmospheric trace species, and additional catalysts threaten to change stratospheric ozone concentrations. Among others is the contention that:

- N<sub>2</sub>O concentrations are increasing as a result of usage of fertilisers
- Cl and Br are released in the stratosphere due to the CFCs usage
- Br is released in the stratosphere as a result of CH<sub>3</sub>Br use in agriculture

In addition, mid-latitude ozone loss has been attributed to different origins:

- in situ depletion from HO<sub>x</sub>, NO<sub>x</sub>, ClO<sub>x</sub>, or BrO<sub>x</sub> chemistry
- transport of low ozone air from the polar vortex
- dilution of low ozone air masses after the break-up of the polar vortex

Also, other effects, apart from the possible chemical destruction, have been under investigation as culprits of ozone reduction:

- natural dynamic variability
- solar cycle (1-2 %)
- quasi-biennial oscillation (QBO), about 1-5 %
- changes in transport patterns

## **2.2 Tropospheric Chemistry**

The troposphere, the lower atmosphere (below about 15 km altitude), is so called because of its turbulent air motions. A boundary layer of about 1 km thickness is often envisaged as an interface between the earth's surface and the free troposphere. The troposphere is characterised by a general decrease in temperature with height to about 15 km. Above this, in the lower stratosphere, the temperature increases with height, the changeover region being known as the tropopause.

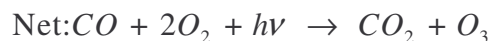
Tropospheric chemistry, on one hand, refers to the chemical processes occurring in the troposphere by which trace substances released into the atmosphere from natural and anthropogenic sources are oxidised. A factor important in tropospheric chemistry is the relatively high concentration of water vapour. In the stratosphere the chemistry involves the reactions that form and destroy ozone in a similar manner ozone formation and removal is

central to the chemistry of the troposphere. The gas-phase chemistry involves the oxidation of organic molecules in the presence of oxides of nitrogen under the actions of sunlight.

The troposphere contains an enormous range of inorganic and organic trace substances. Natural processes release many of them, such as methane, nitrous oxides, dimethyl sulphide. Many, such as the nitrogen oxides, a variety of volatile organic compounds (VOCs) and sulphur dioxide are released by human activities. Others, such as ozone, carbon monoxide and nitric acid, are formed in the atmospheric oxidation of the compounds released from both natural and anthropogenic sources.

### **2.2.1 Tropospheric Ozone production**

Photolysis of  $\text{NO}_2$  is the only known way of producing ozone in the troposphere (Wayne, 1991) since the UV light below 240 nm necessary to photolyse  $\text{O}_2$  cannot penetrate into the troposphere. This is due to the complete absorption by  $\text{O}_2$  ( $< 242$  nm) and  $\text{O}_3$  ( $240$  nm  $< \lambda < 290$  nm) in the stratosphere. Therefore, except for urban areas during pollution episodes, it was commonly assumed until the late 1970s that tropospheric ozone originated in the stratosphere (Junge, 1963). It was believed that stratospheric ozone was mixed through the tropopause region exhibiting a gradient towards the earth's surface which was thought to be the dominant sink. Fishman and Crutzen (1978) compared tropospheric ozone concentrations in the two hemispheres with the then known source and sink mechanisms. It turned out that only about 50 % of the tropospheric ozone has its origin in the stratosphere and is transported through the tropopause. Instead, as proposed by Fishman and Crutzen (1978), the production of ozone in the troposphere is driven by  $\text{NO}_x$  chemistry and reactions involving methane or higher hydrocarbons. The  $\text{NO}_2$  is produced by the oxidation of  $\text{NO}$  by the peroxy radicals, linking hydrocarbon oxidation with ozone production:



Similar schemes can be written using other peroxy radicals  $RO_2$ . Each molecule of CO can create one ozone molecule while each molecule of  $CH_4$  creates 3.5 ozone molecules.



At low  $[NO] / [O_3]$ , ozone loss can dominate ozone production, therefore,  $NO_x$  concentrations determine if ozone builds up or is destroyed at a certain level of hydrocarbon.

### 2.2.2 Photochemical air Pollution; Summer Smog

In remote locations on earth, largely free from man's emissions and with their dependence on the concentration of  $NO_x$  ( $< 1$  ppb), trace substances are still oxidised. However, little ozone is formed photochemically. Instead the peroxy and other radicals may react together, rather than with NO, and form organic peroxides, hydrogen and other compounds, that may be rained out or deposited directly into the biosphere. In the free troposphere in the northern hemisphere, above the boundary layer, the volume ratio of ozone varies between about 30 ppb in winter to 60 ppb in summer. The concentration levels appear to have more than doubled in

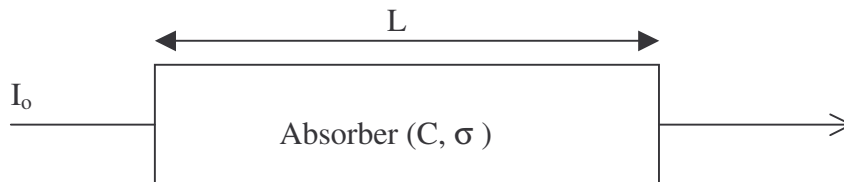
the last hundred years, with most of the increase being attributed to man's activities. The additional ozone is formed photochemically, as shown above (equation 2.2.1b), either in the free troposphere itself or in the boundary layer, from which it is transferred up by vertical mixing. As in remote areas the  $\text{NO}_x$  concentrations in the free troposphere are generally low, so that hydrogen peroxide and other compounds are formed from traditional reactions of the peroxy and hydroperoxy radicals (*Borrell, 1998*).

In the polluted boundary layer, the concentrations of the primary pollutants (by direct emissions,  $\text{SO}_2$  or  $\text{NO}$ ), VOCs and  $\text{NO}_x$  emitted by traffic and industrial sources, are much higher than in the free troposphere above. In the presence of sunlight, high concentrations of ozone and other photo-oxidants are produced, with ozone volume ratios reaching 400 ppb in bad cases. The resulting condition is known as photochemical smog. It was first characterised in Los Angeles in the nineteen fifties, and is prevalent in cities that have a warm sunny climate. The pollutants are trapped within the boundary layer under a meteorological temperature inversion (temperature increasing with height). The high pollutant concentrations facilitate rapid photochemistry and the inversion prevents the polluted air from being diluted by mixing with 'cleaner air' from above. The growth in population and traffic throughout the world means that most sub-tropical and tropical cities suffer from chronic smog conditions. Summer smog episodes are also regional scale phenomena in the populated temperate parts of the world during sunny periods accompanied by stagnant high pressure conditions. It is, therefore, of no surprise that research is being vigorously pursued in all the areas related to tropospheric chemistry in a bid to supporting modern policies for air pollution abatement.

### 3 DOAS Measurement Techniques

Since the 1920s air quality monitoring has been carried out by using spectroscopy. These methods are used for the remote sensing of the atmosphere and thus provide better estimates of the average pollutant concentrations over a given region or area. Ground-based spectrometers equipped with diode array detectors (now replaced by CCD detectors as an optimal option) have been selected as an integral part of the Network for the Detection of Stratospheric Change (NDSC), a collection of strategically placed remote-sounding stations (Kurylo 1991). Differential Optical Absorption Spectroscopy has shown its potential in particular by the detection of different halogen and nitrogen compounds.

The fundamental principle underlying absorption measurements is the Lambert-Beer law: the attenuation of monochromatic radiation is related to the number of absorbing molecules in the optical path,



$$I = I_0 e^{-\sigma LC} \quad (3.0)$$

where  $I_0$  is the incident flux,  $I$  the measured flux,  $\sigma$  the absorption cross section of the species,  $L$  the distance over which the absorption takes place, or optical path length and  $C$  is the concentration of the absorbing species (or density).

In the case of laboratory studies, measurement of the light intensity in the absence ( $I_0$ ) and presence ( $I$ ) of the species of interest is readily applied to obtain concentrations using Equation 3.0. However, the fact that so many species in air absorb in the UV and visible region presents a limitation in that one must be able to distinguish various species from each other as well as from background broad absorption and Rayleigh and Mie scattering of light by gases and particles. This calls for the need to modify the Beer's law. Consequently, UV-visible spectroscopy is, in practice, applied in air only to those species with banded structures ('fingerprints'). To be able to carry this out the differential optical absorption spectrometry (DOAS) technique was introduced (Platt 1994; Plane and Smith 1995).

### 3.1 The Dobson's Equation

The basic idea pioneered by Dobson in the 1930s in designing the famous Dobson total ozone spectrophotometer: the total atmospheric abundance of  $O_3$  can be derived from a measure of the relative intensities of the solar light at two (or more) UV wavelengths (Dobson, 1968).

$$I = I_0 \exp\{-[\alpha X\mu + \beta M + \delta A]\}$$

$$I' = I'_0 \exp\{-[\alpha' X\mu + \beta' M + \delta' A]\}$$

Ratioing, taking logarithm and regrouping terms yields:

$$X = \frac{N - (\beta - \beta')M - (\delta - \delta')A}{(\alpha - \alpha')\mu} \quad (3.1)$$

$N = \ln\left(\frac{I}{I'_o}\right) - \ln\left(\frac{I}{I'}\right)$  is the N factor relating to the O<sub>3</sub> absorption affecting the relative

intensities at the pair of wavelengths, where  $\beta$  is the Rayleigh scattering,  $\delta$  the aerosol term,  $\alpha$  the absorption coefficient,  $\mu$  the geometric airmass factor and X the total column.

The extension of the differential absorption method to other trace species than O<sub>3</sub> triggered the development in the 1980s of low-noise multichannel array detectors having full spectral information available with high signal to noise (S/N) ratios ( $>10^4$ ). Thus the principle of the modern (spectral) DOAS may be summarised in the following equation:

$$I(\lambda) = I_o(\lambda) \exp(-\tau_{Rayleigh} - \tau_{Mie} - \tau_a) \quad (3.2a)$$

$$\ln I(\lambda) = \ln I_o(\lambda) - \tau_{Rayleigh} - \tau_{Mie} - \tau_a \quad (3.2b)$$

where  $\tau_a$  refers to the structured component ( $\tau$  is the optical density) and the rest of the factors of the right hand side of the equation relates to the broadband, which can be approximated by a smooth function of  $\lambda$  (for example, polynomial). A common problem in the analysis of DOAS is due to the occurrence of structures other than noise in the residual of the fit. These structures may indicate an unknown absorber or can be caused by the instrument itself and occur randomly in most of the cases. Stable residual structures cause systematic errors in the analysis which cannot be described by statistical methods.

### 3.2 Differential Cross-sections

Although not absolutely needed, it is a usual practice to use differential cross-sections obtained by separating the low frequency part from the high frequency part of the cross-sections, that is

$$\sigma(\lambda) = \sigma'(\lambda) + \sigma_{\text{broadband}}(\lambda) \quad (3.3)$$

This results in modifying the DOAS basic equation in the form as

$$\ln I(\lambda) = \ln I_o(\lambda) - P(\lambda) - \sum_i \sigma'_i(\lambda) S_i \quad (3.4)$$

where  $P(\lambda)$  is the polynomial (accounting for scattering – Mie and Rayleigh scattering and instrumental effects and  $\sigma_{\text{broadband}}$ ),  $\sigma'_i$  the differential cross-section of species  $i$  and  $S_i$  is the slant column of species  $i$  (the trace gas concentration integrated along the light path).

The actual DOAS retrievals in practice are often complicated by the need to account for additional effects which might be application-specific. One common and very usual problem found in practice is the need to account for inaccuracies or instabilities in the wavelength registration of both laboratory cross-section data and measured spectra, which leads to a slight modification of the DOAS equation:

$$\ln I(a + b\lambda) = \ln I_o(\lambda) - P(\lambda) - \sum_i \sigma'_i S_i \quad (3.5)$$

where  $a$ ,  $b$  are shift and stretch parameters simultaneously fitted, together with  $S_i$  and polynomial coefficients, in a non-linear least-squares process. Similar shift and stretch parameters may have to be considered for the  $\sigma'_i$  as well. The normal practice for the spectral analysis is to take literature cross-sections and convolute it with the respective instrument function (slit function). In particular, the effective absorption seen in zenith-sky radiances corresponds to a complex combination of photons having travelled through a scattering and or absorbing atmosphere. Strictly speaking the DOAS method is only applicable if the effective photon path-length through the absorbing layer of interest does not vary too much with

wavelength (true for an optically thin atmosphere). The zenith-sky equation may be written as:

$$\ln I(\lambda) = \ln I_o(\lambda) - P(\lambda) - \sum_i \sigma_i'(\lambda) V_i \cdot \text{AMF}_i \quad (3.6)$$

where  $\text{AMF}_i$  is the airmass factor which represents the optical pathlength in the atmosphere (enhancement factor) calculated by using a radiative transfer model (RTM),  $V_i$  the vertical column of the absorber and is calculated by dividing the slant column by the appropriate AMF.

### 3.3 Off-Axis against Zenith-Sky Measurements

The measurement of trace stratospheric constituents such as ozone and nitrogen dioxide by means of DOAS is a well-established and widely employed technique. Traditionally, ground-based or airborne measurements employing a zenith-sky viewing geometry have been made, but more recently DOAS has been successfully applied to nadir-viewing instruments on aircraft (McElroy et al, 1999) and satellite (Burrows et al, 1999) platforms. Ground-based zenith-sky observations are made at numerous sites around the world to furnish information about ozone trends and the processes that influence its abundance. Measurements at key sites are performed as part of the NDSC, which coordinates and collates observations. In addition to the quality of the measured spectral data, the accuracy of  $\text{O}_3$  and  $\text{NO}_2$  vertical columns derived from zenith-sky measurements is dependent on how well the transfer of radiation through the atmosphere can be modelled. While interpreting direct solar measurements is relatively straightforward (because the light travels along a single optical path), the analysis of zenith-sky viewing observations necessitates a more complex treatment. Instruments employing zenith-sky viewing geometry receive sunlight scattered from a range of altitudes along a random-walk path. Furthermore, because the intensity measured at the ground varies

exponentially with optical depth, the total slant column is not the sum of effective slant columns for different scattering altitudes.

Scattered sunlight observed at twilight traverses a much longer stratospheric path than scattered sunlight observed at noon. As a result, the apparent slant column density of any species having a maximum concentration in the stratosphere (for example O<sub>3</sub> and NO<sub>2</sub>) is much greater in twilight spectra than noon spectra. For instance, the calculated O<sub>3</sub> optical depth (at 510nm) is typically 16-17 times greater at a solar zenith angle (SZA) of 90° than if the sun was directly overhead (SZA = 0°) (Sarkissian et al., 1995). Vertical column amounts of stratospheric species can be deduced by comparing the observed slant column densities with an appropriate enhancement factor, referred to as air mass factor (AMF), which are calculated with radiative transfer model.

Historically, the influence of clouds on zenith-sky measurements has been largely neglected, because the geometry of zenith-sky observations dictates that stratospheric pathlengths far exceed tropospheric paths at twilight. Furthermore, for measurements of O<sub>3</sub> and NO<sub>2</sub> taken at a suitable distance (at least 200 km) away from urbanised areas, there is little advection of tropospheric pollution to the observation site and bulk of the absorbing column is located in the stratosphere (Bassford et al., 2001 and references therein).

The off-axis geometry and angle (the angle between zenith and viewing direction) was first introduced by Sanders et al. (1993) to observe OCIO over the Antarctica during twilight by which time the zenith-sky observations had already been performed for many years. The strategy was to observe OCIO in the stratosphere using scattered sunlight as far into the ‘polar night’ as possible. As the sun rises or sets, the sky is of course substantially brighter towards the horizon in the direction of the sun than it is in the zenith. In this way, the light intensity

and, therefore, the signal to noise ratio is improved significantly. Their study revealed that absorption by tropospheric species, for example  $O_4$ , is greatly enhanced in the off-axis viewing mode, whereas for an absorber in the stratosphere, for instance  $NO_2$ , the absorptions for zenith and off-axis geometries are comparable. During the time of the measurements of Sander et al. the existing radiative transfer models did not yet allow the calculation of air mass factors for the off-axis viewing mode, so the measurement could only be treated semi-quantitatively (Miller et al., 1997; Hoenninger, 2002).

The main difference between the slant column change for tropospheric and stratospheric absorbers is that for a stratospheric absorber the absorption increases strongly towards twilight whereas for a tropospheric absorber the signal slightly decreases. Work done by Miller et al. (1997) also reported enhanced morning and evening twilight BrO slant columns which were correlated with surface ozone depletion events. From the twilight behaviour they derived the information that the BrO resides low in the troposphere. Mixing ratios of 13 ppt BrO were calculated based on the assumption that the observed BrO is uniformly distributed in the lowest kilometre. Although this study represents the first boundary layer BrO measurements using scattered sunlight in off-axis viewing mode, it suffered from several problems among which are:

- the stratospheric column could not be separated properly; especially the diurnal variation of the stratospheric column masked the changes in tropospheric BrO.
- the use of twilight slant column density behaviour to identify BrO only works when much more BrO resides in the boundary layer than in the stratosphere.
- when only the twilight BrO slant column densities are used, no sudden changes requiring high time resolution can be monitored.

Recent innovations made to the standard zenith sky DAOS setup to use different line of sights near the horizon as additional light sources, coupled with a highly improved radiative transport modelling (RTM), has the propensity to resolving some of the outstanding questions mentioned above. Wittrock et al., 2002 demonstrated, with results from measurements at different latitudes within BREDOM and interpreted with the full-spherical radiation transport model SCIATRAN (Rozanov et al., 2001), that information about the location of the trace gases in the atmosphere is possible. This will pave the way in investigating the consistency of trace gas column amounts derived from different platforms.

## **4 Instruments and Techniques of Measurements**

The traditional zenith sky DOAS instrument, which has been in operation since 1993 in Bremen, had seen a substantial enhancement to the standard setup. The inclusion of the use of different lines of sight near to the horizon as additional light sources is to distinguish between the stratosphere and troposphere including limited profile information in the boundary layer. In this chapter the features of the instruments-spectrometer, Charged Coupled Device (CCD) and the telescope, and mode of operation of the applied Multiple Axis DOAS (MAX-DOAS) is discussed. Results from the calibration of one of the new instruments using the Andor CCD and LOT Oriel Spectrometer (LOT MS257) are also presented in chapter five

### **4.1 Instrumental Design**

To optimise the instrumental design certain features were taken into consideration in the choice of type of instrument. Optimum resolution calls for the trade-off between resolution and sensitivity. Here the optimum resolution is determined by the width of the molecular absorption structures (typically 0.2 to several nanometres depending on species). There is also always the compromise between Grating and Fourier Transform spectrometers (FTS). Within the framework of this thesis, as discussed shortly, grating spectrometers were used. They have medium resolution with unstable wavelength registration but a high light throughput and its cost is (relatively) low. FTS has a high resolution, accurate wavelength registration but low sensitivity and high cost. Also important is the fact that DOAS measurements are done in the ultraviolet / visible (UV / Vis) spectral regions and grating instruments are ideal for this region whereas FTS are best suited for Infrared (IR) measurements.

Detectors are also another key area of consideration. The qualification for this has almost always been linked to low noise and high sensitivity. Cooled diode-array detectors are known

to have high sensitivity and fast readout. On the contrary, and of prime importance, is the new generation of CCDs. The choice here has been the back-illuminated, UV-enhanced sensitivity, slow readout but with 2D imaging capability paving the way for new applications (Airborne MAX-DOAS, measuring from different viewing directions at the same time).

#### **4.1.1 Spectrometer**

The spectrograph used in the set up for the measurement of the atmospheric absorption spectra is of the Czerny-Turner type, based on the original set up developed by Czerny-Turner (1930). It is composed of two convex mirrors and a plane diffraction grating - used to spatially separate light of different wavelengths in a way replacing prisms in most fields of spectral analysis. Incorporated into this system are two diffraction gratings of 1200 lines / nm and 600 lines / nm with the flexibility of user selection by a system-run programme (Figure 4.1 shows the general layout and major features of the LOT MS257<sup>TH</sup>).

An entrance optics consisting of a quartz lens (for UV sensitivity since a normal glass lens blocks all wavelengths below 350 nm) and a round bundle of 38 individual fibres of length 15 m and 150  $\mu\text{m}$  in size are used. The bundle has at its entrance end circularly disposed fibres with the output end aligned. The quartz fibre bundle, which transmits light from the telescope (described in the next section) to the spectrograph, is mounted in the focal point of the first convex mirror (collimating mirror). The parallel light from this mirror is then dispersed by the plane diffraction grating. The second convex spherical mirror, known as the focussing unit, then focuses the dispersed light onto the detector, which is mounted on the axial port shown in the Figure 4.1 below.

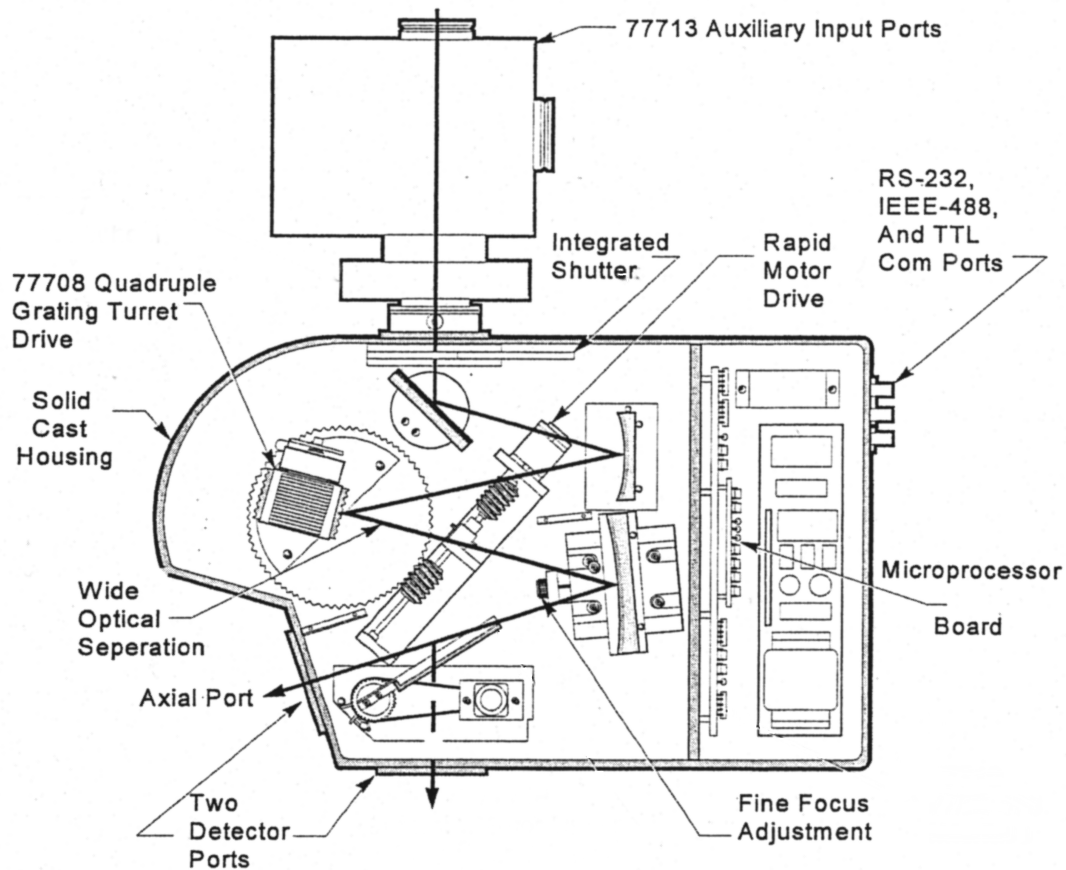


**Figure 4.1** Layout of the MS257<sup>TH</sup>. From Oriel Instruments 77700a-M

The MS257 has an additional capability in use as an imaging spectrograph. This is similar to the conventional spectrograph except that the sources are spatially imaged at the exit plane so that there is a separate spectrum for each input source (applicable to AMAX-DOAS). Great attention has been paid to eliminating straylight. The wide open optical layout and exaggerated tilt of the exit focal plane ensure this. It is important that the diffracted light not be allowed to reflect from the mirrors, or from the face of a focal plane detector such as a CCD, back onto the grating. This light can then be re-diffracted and cause ghost images or straylight at the detector. The spectrograph was designed to remove this possibility for CCD detectors even as large as 28 mm x 28 mm (Oriel Instruments). The straylight is unwanted light which interferes with the light being measured or transmitted. This results in additional

noise to light measurements; at best, incorrect measurements, at worst, the inability to measure any signal.

#### 4.1.2 The CCD

The type used is the back-illumination UV-enhanced for optimal performance in the UV region as shown in Figure 4.4. Andor's DV440-BU CCD is originally designed to offer the best performance characteristics over a wide range of spectroscopy applications. The Andor Technology Limited manufactures tested model DV440-BU, with serial number CCD-2720. The technical specifications are summarised in Table 4.1 below (Andor Technology). The 2048 x 512 array camera is ideally suited to rapid, multi-channel, low-light applications, where high resolution is important.

Number of Pixels	2048 x 512,
Pixel size	13.5 $\mu\text{m}^2$
Format	Back illuminated + UV (350nm) optimised
Active area	27.6 x 6.9 mm
Linearity	Better than 1 %

**Table 4.1** DV440 CCD Specifications

The CCD (detector) is a silicon-based semiconductor chip bearing a two-dimensional matrix of photo-sensors, or pixels. In the high-purity crystalline form, each atom of silicon is covalently bonded to its neighbour. Energy greater than the band gap energy, about 1.1 eV, is required to break a bond and create an electron hole pair. The wavelength of incoming light and photon absorption depth are directly related; the shorter the wavelength, the shorter the penetration depth into the silicon. (Figure 4.2)

## Front and Backside Illuminated CCDs

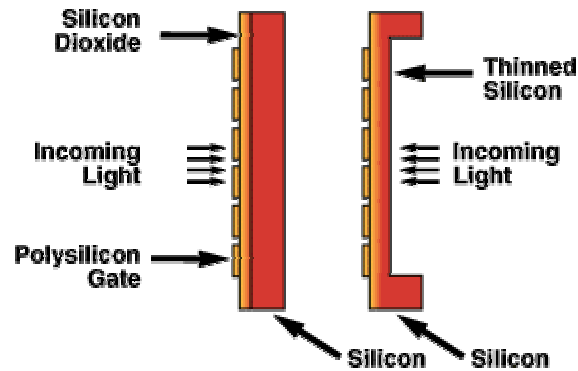


Figure 4.2 Technique for Front- and Back-illuminations

### Typical CCD Chip

Specification (no./size of pixels, etc.) varies according to chip model

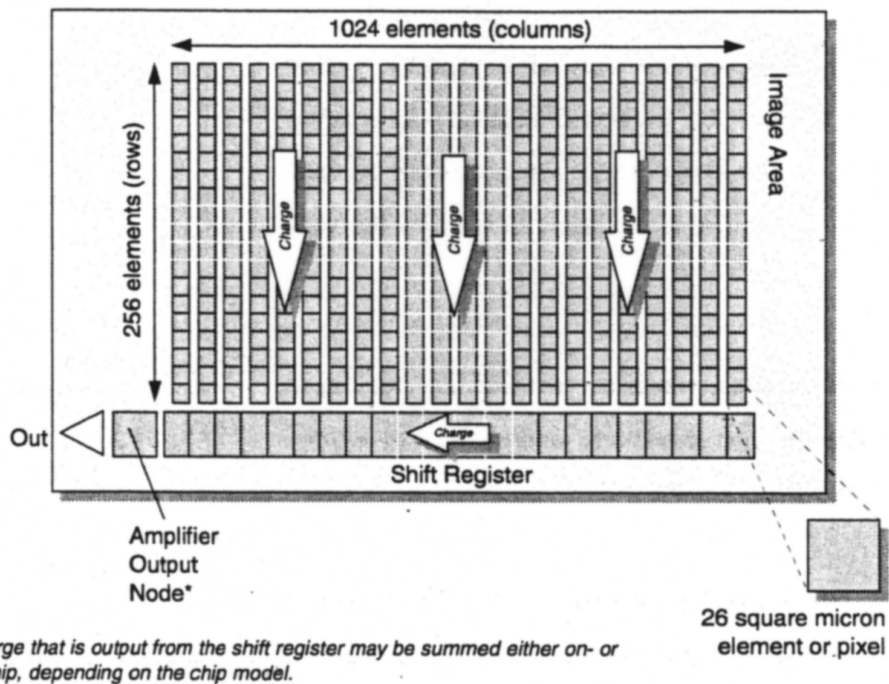
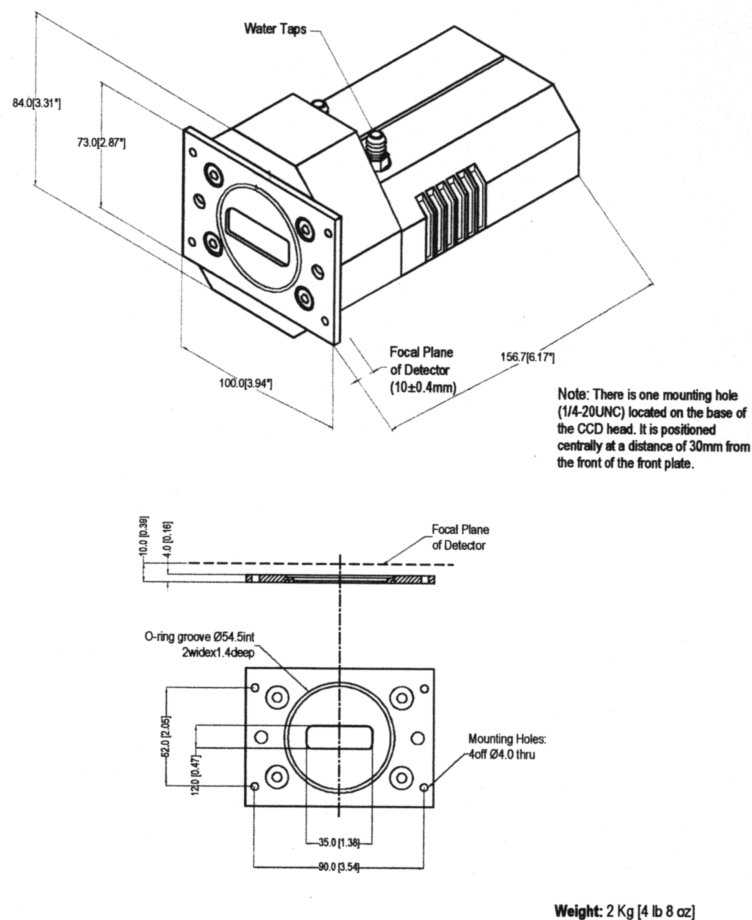


Figure 4.3 Typical CCD chip showing shift registration

Light normally enters the CCD through gates of the parallel register (front-illuminated CCD). These gates are made of very thin polysilicon, which is reasonably transparent at long wavelengths, but becomes opaque at wavelengths shorter than 400 nm. Thus, at short wavelengths, the gate structure attenuates incoming light. To make it applicable to the DOAS

technique (to remove the UV screening), acid-etching techniques are used, to uniformly thin the CCD to a thickness of approximately 10  $\mu\text{m}$  and focus image on the backside of the CCD register where there is no gate structure (back-illuminated CCD, Figure 4.2). Thinned CCDs exhibit high sensitivity to light from the soft x-ray to the near-infrared regions of the spectrum.



**Figure 4.4** Schematic representation of the Andor detector

A typical CCD chip is shown in Figure 4.3 (shift registration), the detector used as in Figure 4.4 (schematic representation). The matrix or the image area has the pixels arranged in rows (running horizontally) and columns (running vertically) comprising 512 rows and 2048 columns. In our case the shift register which runs below and parallel to the light collecting

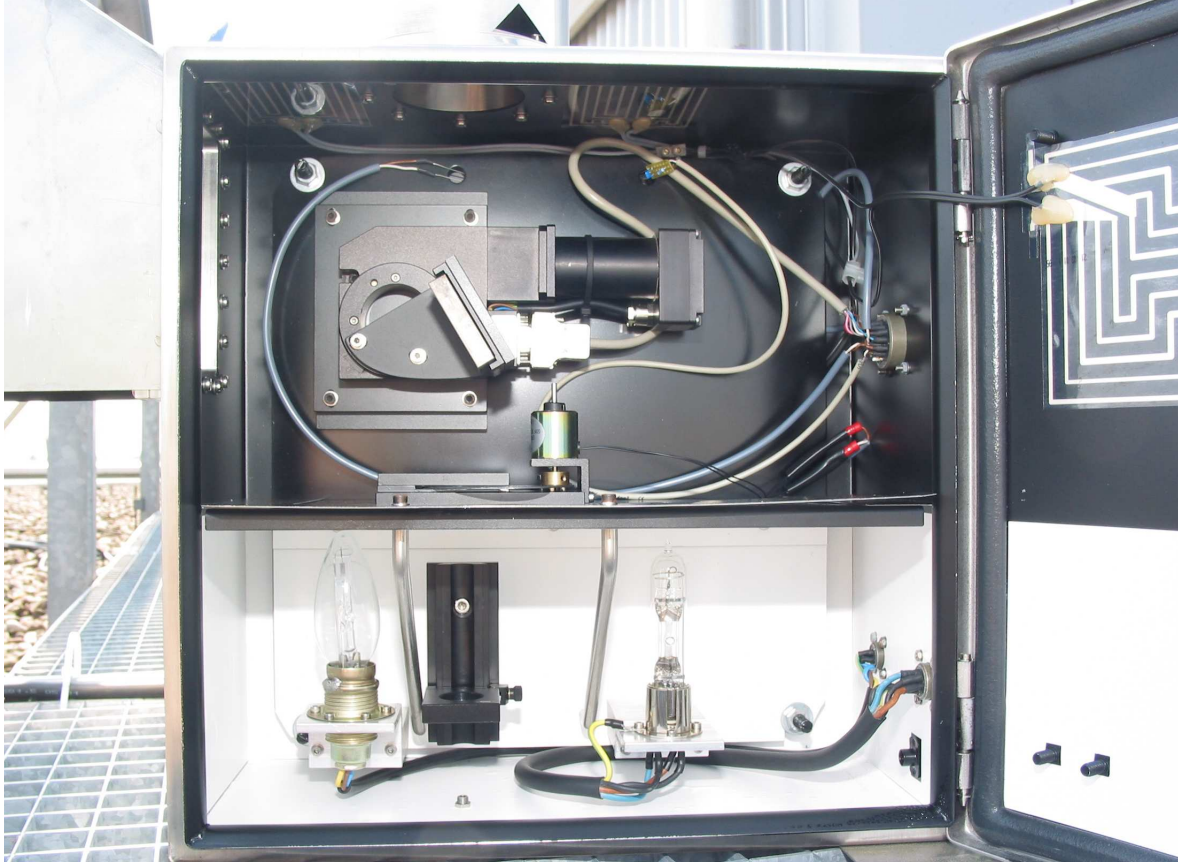
rows, has the same number of pixels as the light-collecting row, but is itself masked, so that no light can fall on it.

### **4.1.3 The Telescope**

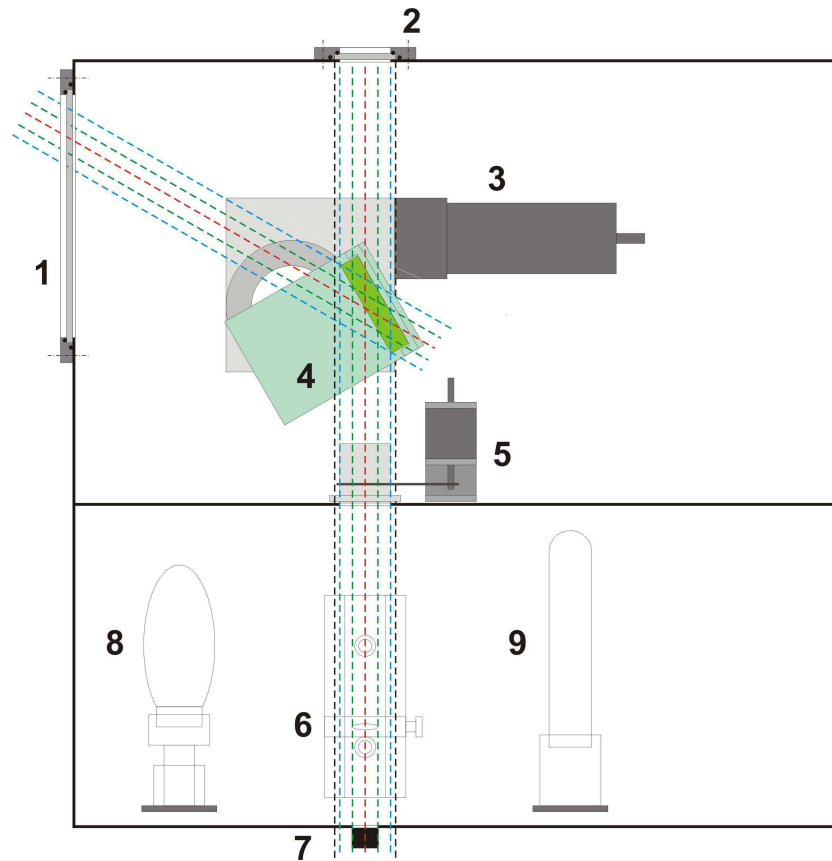
The telescope, which collects the scattered light from the atmosphere via quartz glass windows, was arranged in a dry atmosphere and sealed to prevent contamination and condensation of water on the interior optics. The housing of the telescope is made from a stainless steel and sealed with UV-transmitting quartz windows (both zenith sky and horizon directions) which is designed in such a way to prevent water or snow from accumulating in front of the telescope. Figure 4.5 shows (a) the telescope mounted on the roof - top of IUP Bremen with the door open displaying the internal features and (b) a schematic representation displaying the main features.

Detail description of mode of operation of the various parts are outlined in the next two sections.

(a)



(b)



1. Quartz glass window off-axis; 2. Quartz glass window zenith;
3. Servomotor with rotating stage; 4. Mirror; 5. Shutter; 6. Lens
7. Quartz fibre; 8. Tungsten lamp; 9. HgCd lamp

**Figure 4.5** Telescope showing the main features

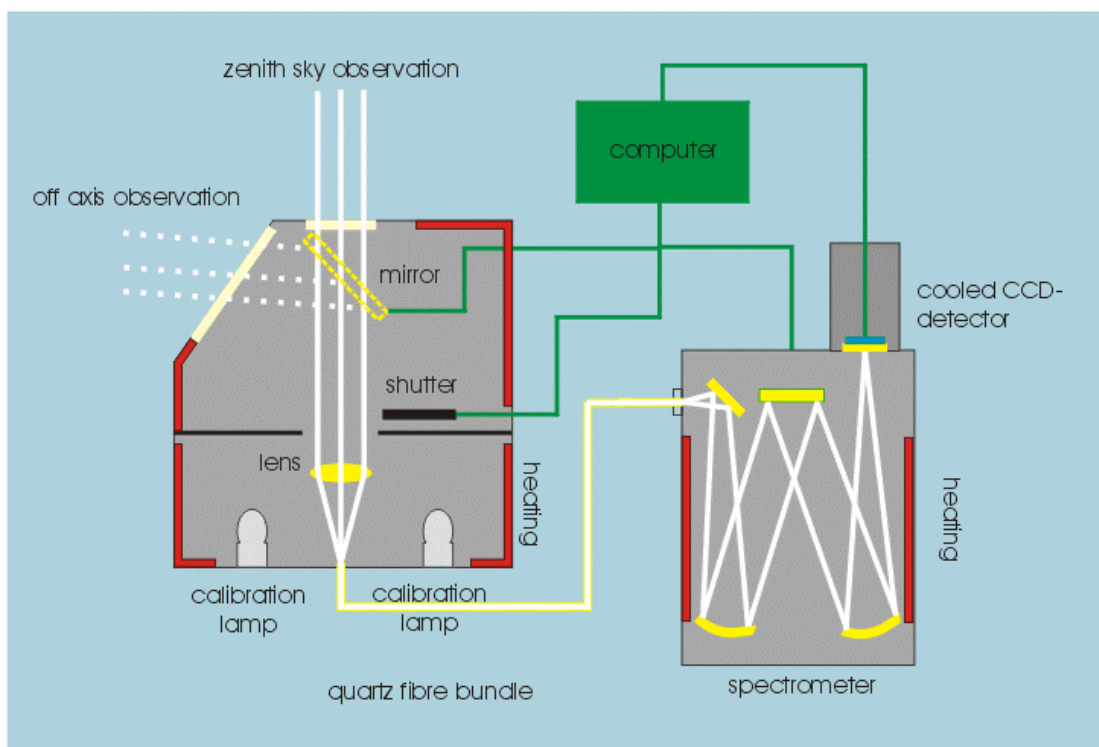
## 4.2 The MAX-DOAS Instrument

The Multi-Axis-DOAS (MAX-DOAS) instrument is a novel development based on a combination of the zenith scattered light DOAS and DOAS observations made for off-axis geometry (Figure 4.6). Simultaneously scattered sky light is observed from different viewing directions. While for different viewing angles the sensitivity for stratospheric absorptions is very similar, those for tropospheric species differ significantly. The smaller the elevation angle is the larger the sensitivity for species located near to the ground. The basic principle is to form the difference of the simultaneously derived trace gas absorptions for selected viewing directions. Thus the (possible) stratospheric contributions cancel out and the derived

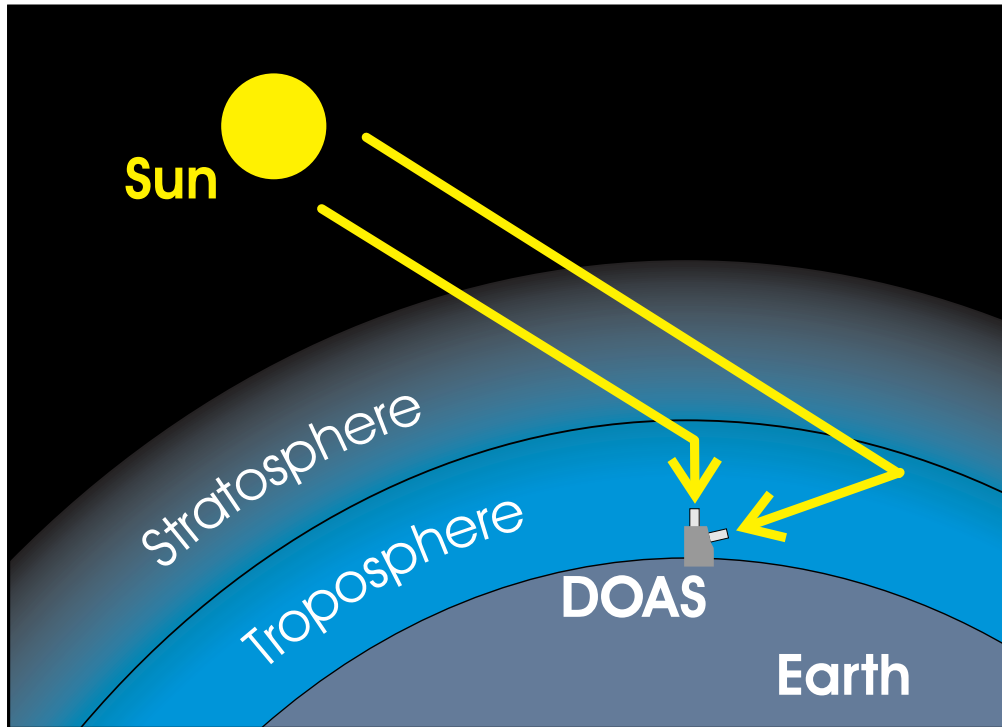
result is sensitive only to the tropospheric absorption. For the quantitative interpretation of the result, however, radiative transfer modelling has to be applied, SCIATRAN (Rozanov et al., 2001).

Figure 4.7 shows how the scattered light from the atmosphere passes through the two layers (stratosphere and troposphere) before being received by the DOAS instrument installed on the ground.

For the zenith sky view, there is a short path traverse by the light through the troposphere but a long path through the stratosphere. On the other hand, when considering the horizontal view, the light traverses a long path through both spheres. By combining results from the different viewing directions, limited profile information can be obtained with the help of a radiative transport model.



**Figure 4.6** Features of the instrumental set-up of Bremen new Generation MAX-DOAS



**Figure 4.7** Light path through the various layers

#### 4.2.1 Mode of operation of the MAX-DOAS

The MAX-DOAS instrument consists of a grating spectrometer, a CCD detector, a telescope, a quartz fibre bundle between the spectrometer and telescope and a computer for data acquisition as shown in Figure 4.6 above. The scattered light from the zenith-sky is collected by the telescope and pass into the grating spectrometer via the quartz fibre bundle. The pointing of the telescope is alternating between the zenith and the horizon. Different lines of sight are realised by a mirror (labelled 4 in Figure 4.5 b) fixed on a rotating stage (Micos DT-80) which is moved by a computer controlled servomotor with integrated motion controller 3 (Faulhaber 3564K024BC). This set-up allows to move the mirror in every needed position with accuracy of  $\pm 0,04^\circ$  and a repeatability of  $\pm 0,008^\circ$ . The instrumental set-up of the telescope is shown in Figure 4.5. In zenith sky mode the lens (6) is directly illuminated. In the off-axis mode the mirror is moved into the light path and reflects the collected light to the

lens. The line of sight of the off-axis measurements is limited by the size of the entrance window (1). Lines of sight from  $-2^\circ$  to  $30^\circ$  are possible.

Relative radiometric response of the instrument and wavelength calibration measurements using a HgCd lamp (9) and a Tungsten lamp (8) are automatically performed every night. During the calibration measurements the lower part of the telescope is closed with a shutter (5) to protect it from atmospheric straylight.

The spectrograph is measuring in the UV / VIS wavelength region 330 – 490nm. For detection, the CCD is used allowing simultaneous measurements over the complete wavelength range. The polarisation response of the grating spectrometer is a potential source of artefact for applications using polarised light sources, for example the zenith sky light. The quartz fibre optic bundle is used to depolarise incoming light.

The entire instrumental set-up is software supported and this makes the operation of the system wholly automatic. The spectrometer is equipped with flat ruled gratings with 600 and 1200 l / mm lines. The choice of which grating in operation is also software supported. The CCD has only the imaging and vertical binning modes supported, even though other modes could equally be supported, as a matter of choice and application. The automatic measurements mode is used for standard atmospheric measurements. It is intended for operating the instrument automatically over a long time period without user interference. During automatic measurements,

- measurements are taken within a fixed solar zenith angle (SZA) range
- exposure time is determined automatically using a test measurement prior to each block of measurements

- the mirror of the multi-axis telescope is operated automatically
- manual operation of lamps and telescope shutter is disabled (further details may be found in AMAX\_OMA Manual Version 1.8, for internal circulation only).

In a standard operation mode, the signal is integrated vertically resulting in a single spectrum with high S / N ratio. A shutter situated in front of the CCD is automatically opened during measurement and closed during read-out of the detector. In automatic operation, the integration time is determined from a short test measurement prior to the measurement itself. In manual operation, the optimal time can be determined and set using the menu of the software. The multiple viewing direction ability of the instrument makes it possible to take measurements aimed at both stratospheric and tropospheric absorbers.

To avoid damage to the instrument, a viewing direction must not be used when the sun is entering the field of view of the telescope. In addition, even if the sun is illuminating only the quartz windows at any point without actually being in the field of view of the telescope, straylight deteriorates the measurement quality severely. Also, close to the sun forward scattering of photons is important and makes interpretation of the results difficult. In short, measurements in direction of the sun are to be avoided.

## 5 Calibration Measurements

The need to characterise the detector and the spectrographs is paramount to a good and reliable multi-axis DOAS measurement. It is critical to know very well the properties and the performances of the overall instrument aside the system specifications given by the manufacturers. This includes the readout noise, saturation signal per pixel and dark current, which refers to the leakage of charges into the pixel. For instance, the characterisation of the linearity between light intensity and signal read out will help to establish the upper limits for the useful range of the detector signal. Also, light photons measured by the ground-based instrument undergo scattering with passage through the atmosphere (Mie and Rayleigh scatterings). In effect, polarised scattered light reaches the instrument and as such the polarisation dependency of the instrument has to be tested in order to account for it if necessary. Again, before cross-sections can be made for a particular spectrometer, the instrument transmission with wavelength function, hereinafter called the slit function, of the spectrometer is required. For DOAS, the most important input for the fit are the absorption cross-sections of all relevant absorbers in the wavelength region of interest. For an accurate and more reliable cross-section convolution the slit function of the instrument has to be optimised.

The details below give the results of the tests performed in the laboratories of the DOAS-group within IUP, Bremen. Four different measurements were carried out during the calibration exercise of this work as described in the following sections namely: Dark Current, Linearity, Polarisation, and Slit function measurements respectively. The experimental set-up generally used for the entire calibration is shown in Figure 5.1 below.

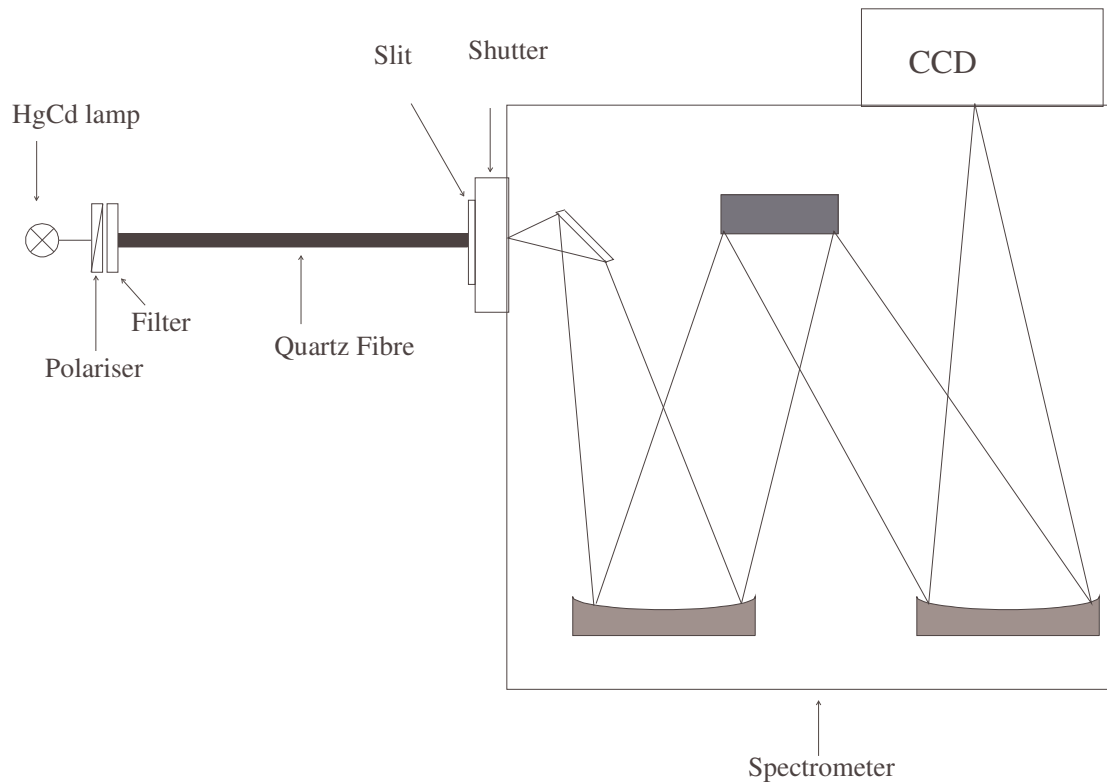


**Figure 5.1** Schematic representation of the set-up in the laboratory of IUP, Bremen

## 5.1 Dark Measurements

The dark measurement is used for characterising the detector readout noise and dark current (leakage of charges into the pixel) as a function of integration time and detector temperature. The offset current, average electronic direct current (DC) for the CCD at the minimum exposure time under dark conditions is to be determined. The dark signal is produced by the flow of dark current during the period which the CCD collects light prior to readout. Thus, all CCDs produce a dark current, an actual current that is measurable in (typically tenths of) milliamps per pixel. It adds to the measured signal level and increases the amount of noise in the measured signal. It varies with temperature causing background values to increase over time (A user's guide to Andor CCDs). That is, for a given temperature the actual dark current can vary by more than an order of magnitude from device to device. The devices are specified in terms of minimum dark current achievable rather than minimum temperature. Although

dark current is not the main error source in DOAS measurements, reducing the temperature of the chip is important to reduce the impact of hot and bad pixels present on each CCD.

The experimental set-up used is as shown in Figure 5.1 above without the quartz fibre, filter, polariser and the lamp. The laboratory was kept dark with the spectrometer well shielded against any external light sources whilst the shutter was closed. The dark signal depends on the temperature of the CCD so measurements were performed at varying temperatures from – 55 °C to –20 °C for CCD 2720 and –45 °C to –20 °C in the case of CCD 2722 with the interval of 5 °C. The exposure times range between 0.02 and 1638 seconds. In the first instance, the dark signal was averaged over 20 measurements for exposure times less than 100 seconds and averaged twice for the exposure times between 100 and 1640 seconds (for CCD 2720). During the subsequent measurements for the second CCD 2722 the entire measurements were averaged over ten for all exposure times. In all the cases, the exposure time and the CCD temperature were varied as summarised in Table 5.1 below.

<b>CCD</b>	<b>Exposure Time/sec</b>	<b>Temperature / °C</b>	<b>Dark Average</b>
2720	0.020, . . . , 86.02	-20, . . . , -55	20
	176.04, . . . , 1376	-20, . . . , -55	2
2722	0.025, . . . , 1638	-20, . . . , -45	10

**Table 5.1** Table of measurements performed

The signal was saved in two modes, imaging and vertical binning, 512 x 2048 pixels and 2048 pixels respectively. In the analysis the spectrum was used, by averaging for a given exposure time and CCD temperature. Spikes caused by cosmic rays were deleted from the spectrum before taking the average to ensure that only dark signals are taken into account.

The final signal variations are shown in Figure 5.2 and Figure 5.3 for the CCDs 2720 and 2722 respectively. Figure 5.2 is obtained by subtracting constant values of 10 to 40 count /

pixel in the steps of 5 count / pixel from the original values for each corresponding temperature starting from  $-25\text{ }^{\circ}\text{C}$  to  $-55\text{ }^{\circ}\text{C}$  respectively. The values for  $-20\text{ }^{\circ}\text{C}$  were kept constant in order to act as a baseline for deductions. In this way the points, which were almost lying on each other for exposure times below 100 seconds, were spread out nicely for closer and easy identification.

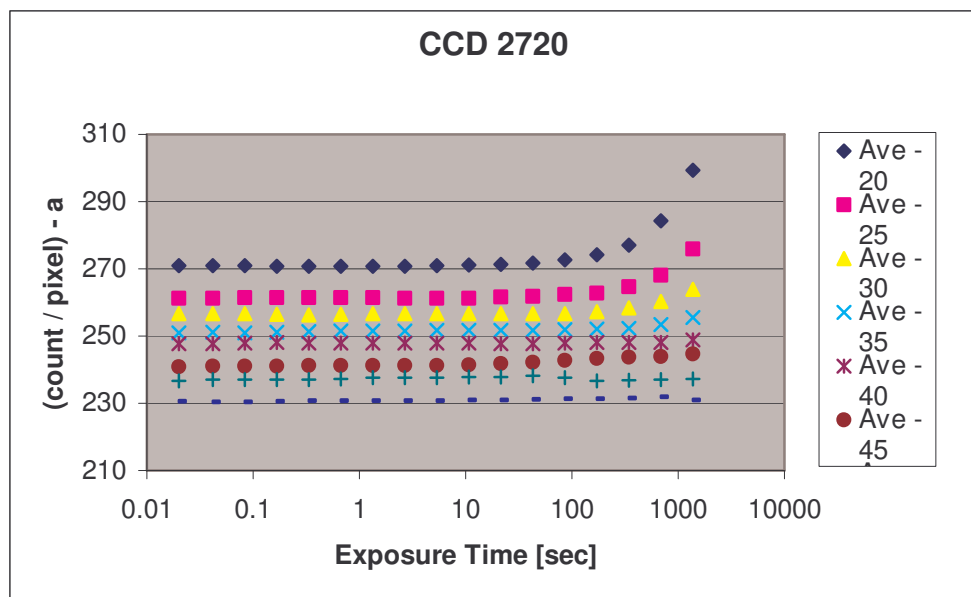


**Figure 5.2** Dark signal variation as a function of exposure time and CCD 2720 temperature

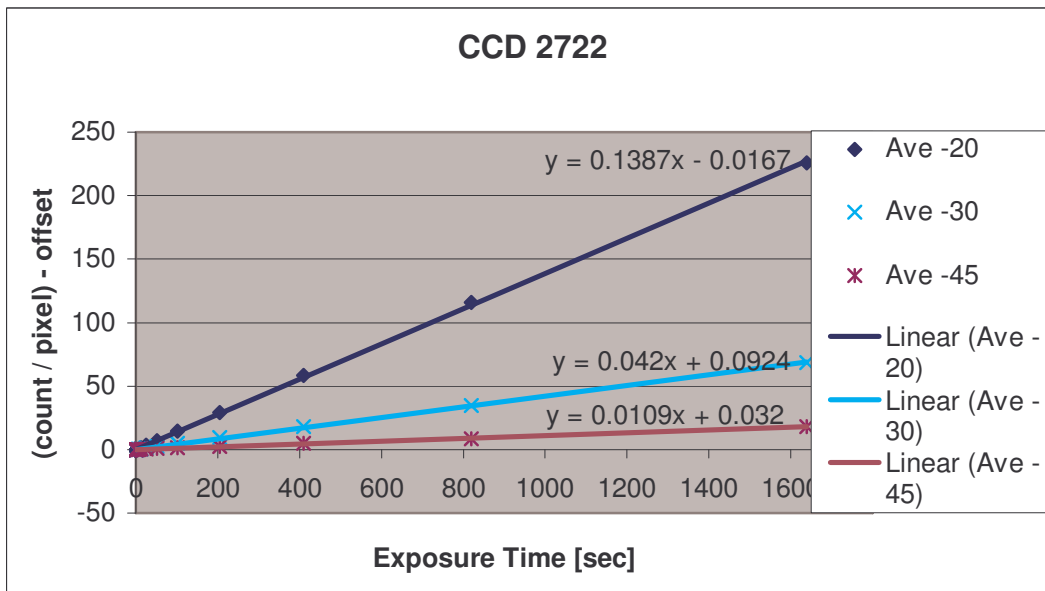
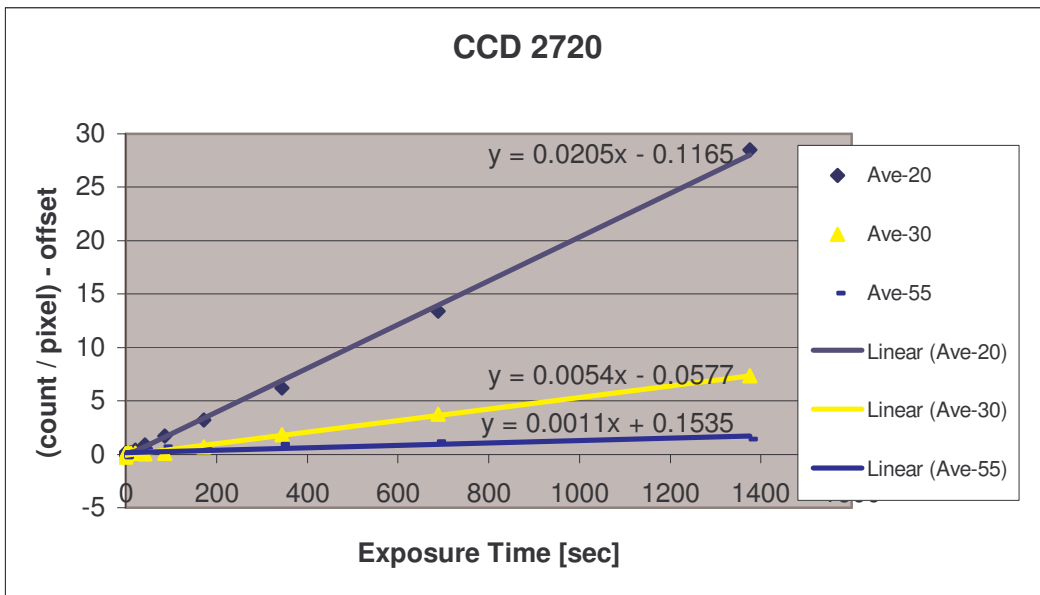


**Figure 5.3** Dark signal variation as a function of exposure time after offset correction.

A similar procedure was carried out for CCD 2722 (not shown here since a similar trend is observed). Also, the offsets for both CCDs were plotted against the temperature by taking the mean values for exposure times between 0.02 and 11 seconds. Figure 5.3 shows the result of deducting the offset from each signal and for all temperatures with only three typical temperatures shown here as a case study. This enables the final dark current uniformity estimation plot to be realised as in Figure 5.4 by plotting the slope against the temperature. The general trend seems quite similar in both cases. The Figures have different colours and

marks referring to different CCD temperatures. It is seen that the dark signal shows no tremendous changes with temperature at exposure times below 100 seconds. When the exposure time is longer the signal increases reasonably by some counts with increasing temperature. For instance, CCD 2720 has a change of nearly 30 and 10 count/pixel for  $-20$  and  $-25$  °C respectively (Figure 5.2). Obviously the signal at low temperature is much smaller and as a result its change is also smaller.

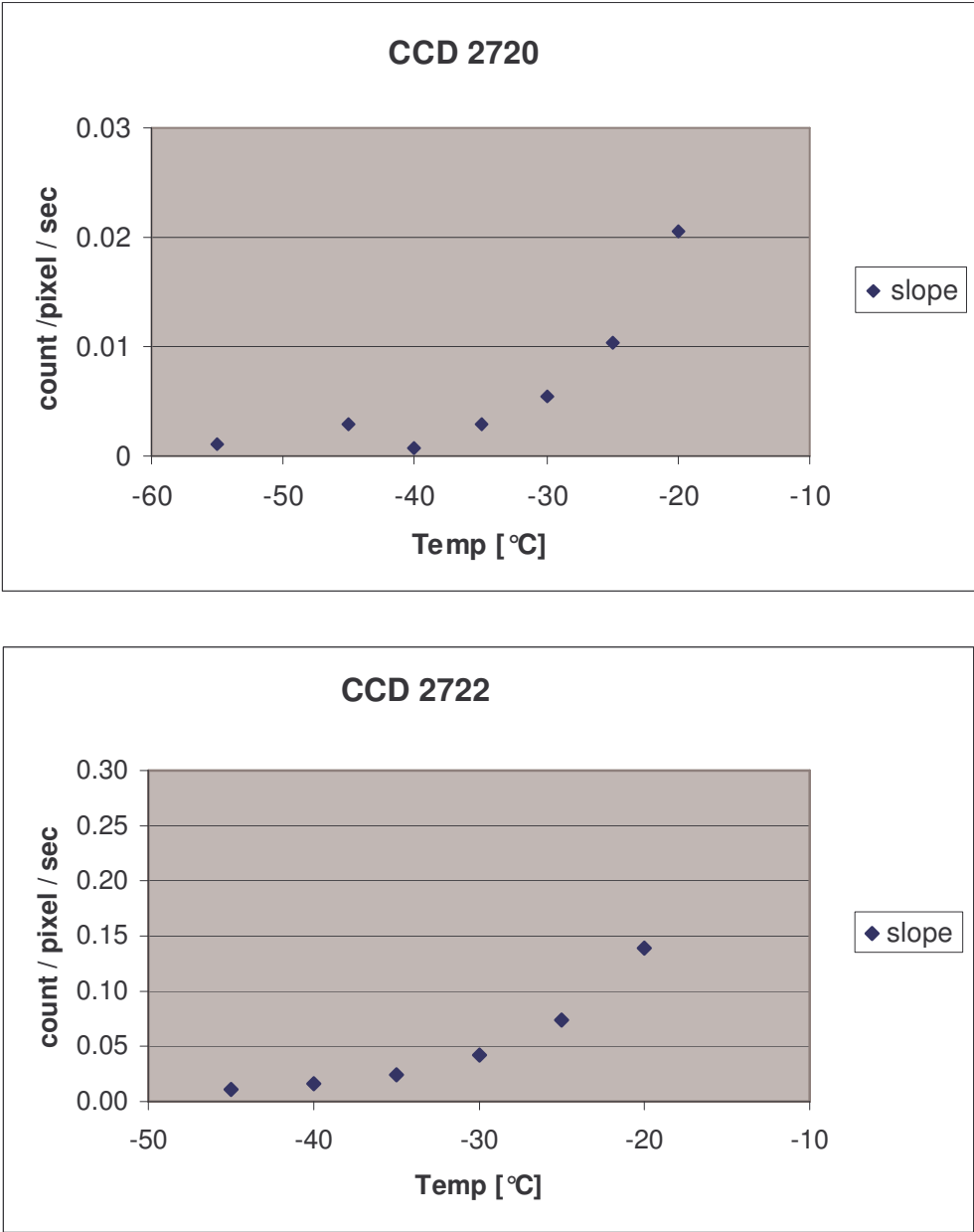


**Figure 5.4** Dark current for the two CCDs

The Figures show that with increase of CCD temperature the dark signal appreciably increases. More clearly seen is the increase of dark signal with temperature for exposure times above 100 seconds.

### **5.1.1 Explanations**

A large offset that is found in the case of CCD 2722 and this is attributable to the time taken for the cooling and running of the CCD. That is the time interval for taking the readings and cooling down of the detectors were not the same and this has an influence on the offset. It is observed that for exposure times less than 100 seconds the dark signal is quite negligible and this could be the safe range for operating the detector. Also, lowering the temperature of the CCD lowers the dark signal (Figure 5.3 and Figure 5.4). For CCD 2720 the dark current uniformity is about 0.003 count / pixel / sec (about 0.3 counts). Clearly  $-40\text{ }^{\circ}\text{C}$  may be recommendable operating detector temperature ignoring all probable inherent errors in the CCD. On the other hand, CCD 2722 shows a dark current uniformity at about 0.03 count / pixel / sec (about 3 counts). This is a bit on the higher side than CCD 2720 and the  $-40$  and  $-45\text{ }^{\circ}\text{C}$  prove to be a reasonable operating temperature for this detector. In effect, the reproducible increase in the dark signal with decreasing CCD temperature may be attributed to some degree of dependence on the offset.

The general impression, as shown from the Figures above, is that  $-45\text{ }^{\circ}\text{C}$  and  $-40\text{ }^{\circ}\text{C}$  CCD temperatures are more favourable range for operating the detectors. Dark signal correction for all integration times less than 100 seconds at  $-40\text{ }^{\circ}\text{C}$  and  $-45\text{ }^{\circ}\text{C}$  may be neglected within the limit of this investigation. Again, it is realised that fast particles create random signals on the CCD with frequency of one event every few seconds and using a long exposure time will accumulate many such events.

## 5.2 Linearity Measurements

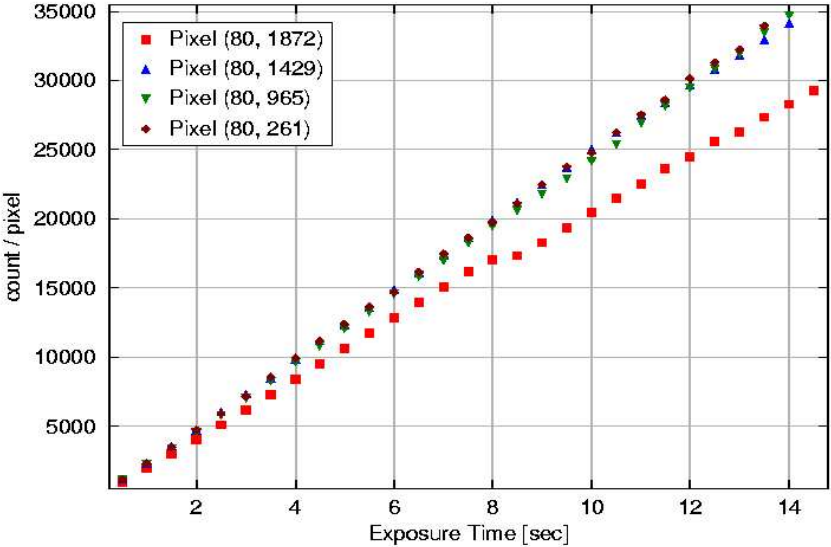
The signal measured in counts by the detector, after dark signal correction, is proportional to the light intensity falling on the CCD chip. It is the direct representation of the light photons collected by the telescope from the atmosphere. The limits for the useful range of the detector signal read out across the chip have to be well established in ensuring good measurements. The linearity of a detector is expressed as the percentage deviation from a straight line fit. Several scans of the Tungsten lamp (a stabilised white light) were performed with increasing integration times from 0.5 to 15 seconds at the steps of 0.5 seconds without using the quartz fibre (Table 5.2). The measurements were performed with the spectrometer set to the operational wavelength region of 320 nm to 420 nm and a detector temperature of 40 °C.

Maximum Intensity at Column	Row			Exposure Time / sec
	80	250	510	
261, 965, 1429, 1872				0.5, 1.0, 1.5, ... , 15

**Table 5.2** Table showing Linearity measurements taken using the CCD 2720

The set-up is the same as in Figure 5.1 but this time the polariser, and quartz fibre were removed and the HgCd lamp replaced by a Tungsten lamp. Prior to the measurements, the lamp is switched on and the programme is allowed to wait for some time, about 15 minutes, until the lamp has stabilised. The position of the lamp is maintained throughout the measurements to ensure nearly constant light intensity. The shutter to the spectrometer is also opened. The spectrum was measured with the filter UG11 that has two transmittance windows, one from 200 to 400 nm and the second from 700 to 900 nm. This offers the possibility to scan through the entire chip covering all the possible wavelengths. The centre wavelength was changed each time a scan is taken for any part of the chip (left, middle and right part of the chip).

Figure 5.5 shows the counts per pixel as a function of exposure time. The various positions on the chip go into saturation at different counts. In the Figure 5.5 two different lines (80 and 510) on the chip were chosen for four different columns to ensure that the entire chip is fully scanned. At 16 and 26 kilocounts, the lower part reaches saturation whilst the upper part goes beyond 35 kilocounts. By definition the linearity is expressed as a percentage deviation from a straight line fit and from the Figure after 2 and 4 seconds respectively for the lower and upper parts the lines deviate by several counts. This represents a percentage higher than 1 % making the detector a suspect and further testing was recommended.



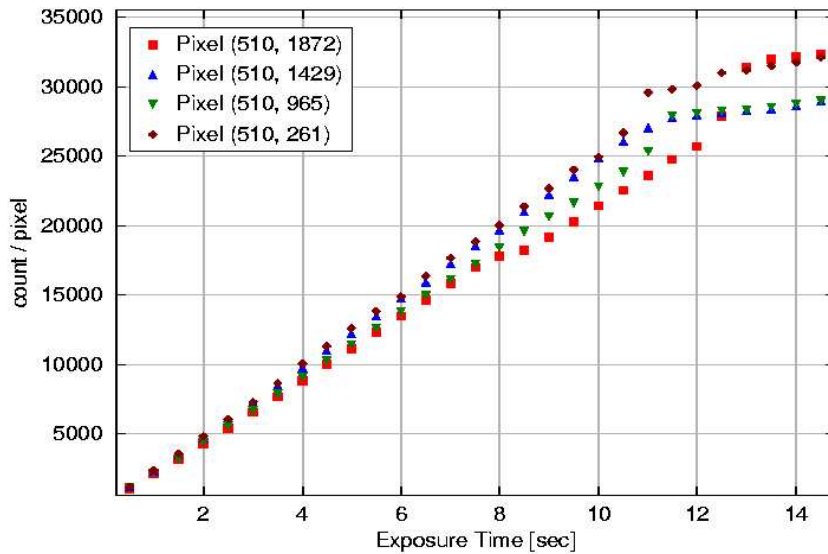


**Figure 5.5** Linearity for various positions and centre wavelengths of the CCD 2720

### 5.3 Polarisation Dependency Measurement

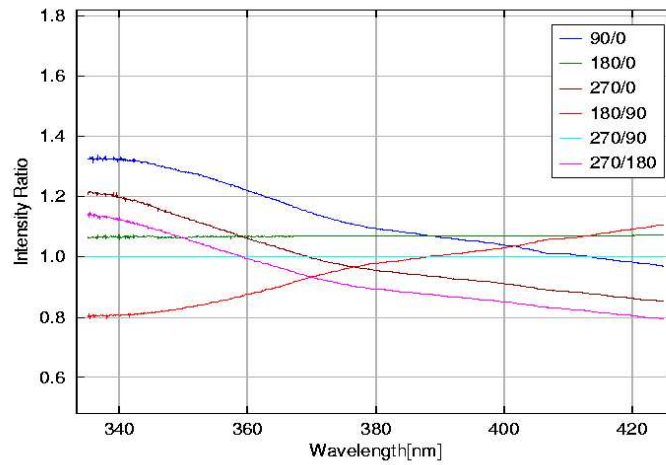
All optical instruments have different sensitivity towards light polarised parallel to the optical axis than towards light polarised perpendicular to this axis. Most of this sensitivity changes slowly with wavelength and is of no concern to the DOAS retrieval. However, some components of the spectrometer exhibit sharp changes in sensitivity for the different polarisations, and introduce wavelength dependent signatures in the measured spectra if not corrected.

To ensure that the spectrometer is measuring the exact atmospheric absorber concentrations over the measurement site in question, the polarisation dependency of the instrument with wavelength has to be tested. The telescope receives scattered light, which is polarised by the air molecules from the atmosphere (Rayleigh scattering). The instrumental polarisation dependency with wavelength must be checked and accounted for if found to have great influence on the quality of the final spectra.

The set-up is the same as in Figure 5.1. Measurements of a tungsten lamp (30V, 60W) were taken with a polariser and a filter FG3 (used to cut off the longer wavelength range, below 530 nm) in the optical axis. First the 600 and 1200 grating lines / nm were used without quartz fibre for the CCD 2720 at  $-40\text{ }^{\circ}\text{C}$  at measurement wavelength region and exposure time of 2 seconds for 10 measurements. The procedure was repeated for the polariser at different positions of rotation namely,  $0\text{ }^{\circ}$ ,  $90\text{ }^{\circ}$ ,  $180\text{ }^{\circ}$  and  $270\text{ }^{\circ}$  respectively. One line lamp and dark measurements were also taken at 0.021 seconds for each grating for calibration purposes.

The measurement is then taken again but this time using the quartz fibre for the two gratings with the polariser and the filter arranged in the optical axis. The quartz fibre bundle delivers the light to the spectrograph. The bundle contains several single fibres, at the entrance end the fibres are disposed circularly whereas they are aligned at the output end. The plot below, Figure 5.6, is representative of the 600 grating lines / nm with and without quartz fibre. It is typically the plot of normalised intensities of the different polariser positions with respect to the orientations as a function of wavelength. It shows clearly that without fibre there is a wavelength dependency whilst by using the fibre there is no eminent wavelength dependency of light intensity for the different polarisation positions of the incident light. The result shows that the quartz fibre is helping in depolarising the scattered light by way of transmitting the light from the focal point of the quartz lens to the entrance slit of the spectrometer.

(a) Without Fibre



(b) With Fibre

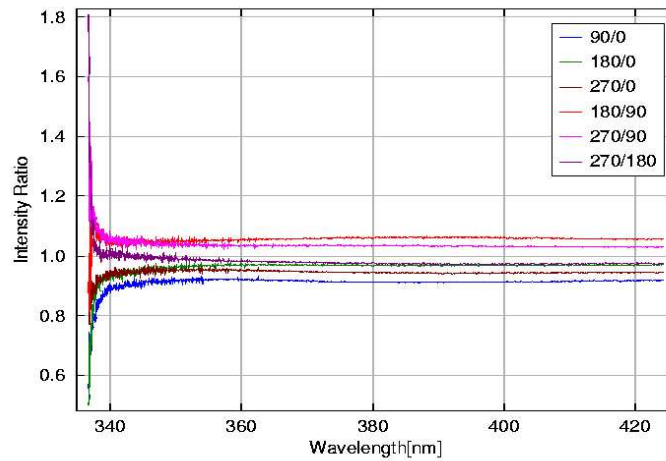


Figure 5.6 Polarisation dependency with wavelength for 600 grating lines

## 5.4 Slit function Measurement

The slit function is the instrument transmission with wavelength function. It is obtained by measuring the spectrum of a line lamp (HgCd lamp) with the spectrometer, and selecting a line that is free from overlap with nearby lines. It is necessary to know the slit function before a convolution of cross sections can be made for a particular spectrometer. Convolution is a useful process because it accurately describes the effects that occur in the spectrometer such as the shape of the spectrum.

Measurements of line lamp (Mercury Cadmium lamp) at different wavelength settings covering the entire CCD chip are carried out with one strong line (404.66 nm) in steps of about 50 pixels (4 nm for 600 grating lines / nm). The lamp is allowed to stabilised before measurement is taken by allowing some time to elapse after switching it on. The wavelength range covered is 320 nm to 490 nm with steps of 4 nm. The instrument is arranged as in Figure 5.1. The light is diffused from the lamp so that the spectrometer's field of view is filled in the same way as when the spectrometer is in normal use (operational mode), to ensure that no inaccurate transmission function results. A 100  $\mu\text{m}$  slit width was used in both cases. Figure 5.7 shows the transmission function derived from the HgCd line spectrum, which has the wavelength axis replaced by a delta wavelength axis relative to the centre of the line.

From the Figure it is evident that there is no appreciable change in the band pass (Full width half-maximum). Nevertheless, it is seen that the asymmetric nature of the shape of the spectrum is not good for an optimal convolution of the cross section of the spectrometer. It is likely to improve on the symmetric nature of the shape by adjusting the spectrum when setting up the instrument for live measurement at the measurement site.

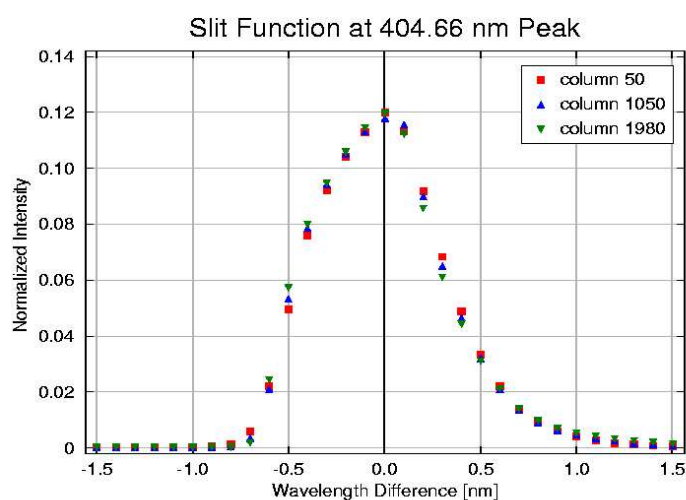


**Figure 5.7** Spectrum of the HgCd lamp obtained on the CCD2720 chip with an entrance slit of width 100  $\mu\text{m}$ .

## 5.5 Summary

In this chapter important properties of the CCD camera (model DV 440-BU from Andor Technology) and the spectrograph (LOT MS257) like the dark current, linearity, polarisation dependency and slit function were investigated. The results show that the CCD camera has a low dark current (about 0.003 count / pixel / sec and 0.03 count / pixel / sec respectively for CCD 2720 and 2722). The linearity is poor and shows a percentage deviation from the linear fit on the higher side ( $> 1\%$ ). Polarisation dependency with wavelength is seen to have been taken care of by the incorporation of the quartz fibre bundles into the set up and need not be considered during the DOAS retrieval process. Finally, the slit function shows a constant band width but the asymmetric nature of the shape requires that the spectrum be readjusted during the set up before any real measurement is taken.

## 6 Data

Ozone data (vertical columns) for the year 2001 from the satellites Global Ozone Monitoring Experiment (GOME) and Earth Probe-Total Ozone Mapping Spectrometer (EP-TOMS) are used. The GOME and TOMS instruments observe the Earth's atmosphere in nadir geometry from a polar, sun-synchronous orbit. The data was then compared with the zenith sky DOAS (described in Chapter 3) ozone data over Bremen in 2001. Some selected data from Bremen and Nairobi MAX-DOAS instruments are also analysed for ozone and NO<sub>2</sub> slant columns in this chapter.

### 6.1 GOME

GOME is a spectrometer on board ERS-2, which was launched on 20 April 1995 and flies in a sun-synchronous, polar orbit at an average height of 785 km above the Earth's surface (Burrows et al., 1999, and references therein). The main target of GOME is the determination of the global stratospheric ozone field. However, the broad spectral coverage and the relatively good spectral resolution also allows for the retrieval of a number of other trace gases that have structured absorptions in the UV and visible wavelength range. Under clear sky conditions, visible and near UV radiation reaches the surface, and provides GOME with a unique sensitivity towards tropospheric absorbers. In particular, GOME measurements have been used to study tropospheric SO<sub>2</sub>, (Eisinger and Burrows, 1998), BrO (Wagner and Platt, 1998; Richter et al., 1998), HCHO (Ladstätter-Weißmayer et al., 1999; Thomas et al., 1998; Chance et al., 2001) and NO<sub>2</sub>, (Leue et al., 2001; Velders et al., 2001).

GOME is a grating spectrometer covering a spectral range from 240 nm to 790 nm. The short-wave region of GOME covers the Hartley-Huggins ozone bands, which contain information about the vertical ozone distribution. The GOME instrument observes in nadir viewing

geometry the light (UV/visible) scattered back from the atmosphere and reflected at the ground. Once per day, it also observes the extraterrestrial solar irradiance. The atmosphere is scanned with a spatial resolution of 320 km × 40 km (across track × along track) (forward scan) and 960 km × 40 km (back scan). Each individual orbit of ERS-2 takes about 100 min. Although the repeating cycle of an orbit is 35 days, nearly global coverage (except for a small gap around the poles) is achieved within three days applying the maximum scan width of 960 km (ESA, 1995). As a result of the sun-synchronous orbit, the measurements in low and middle latitudes are always taken at the same local time (LT) (the northern mid-latitudes are crossed at about 10:45 LT).

The calibration unit on board is adjacent to the spectrometer part consisting of the sun view port and a compartment housing a Pt/Ne/Cr hollow cathode discharge lamp. The solar radiation is attenuated by a mesh (20% transmission) and directed via a diffuser plate (wet-sanded Al plate with Cr/Al coating) on to the entrance slit of the spectrometer. When no solar measurements are carried out and during nadir and calibration lamp measurements, a protective shutter is placed in front of the solar view port in order to avoid unnecessary UV exposure and to prevent straylight from entering the instrument. The calibration unit becomes optically coupled to the spectrometer by proper positioning of the scan mirror (Burrows et al., 1998; GOMEMANNUAL 1995).

The various pointing geometries of the GOME scan mirror permit in addition to solar and earth nadir viewing, polar viewing (scan mirror angle of 45°), and lunar observations (scan mirror angle of about 80°) at selected times during a year.

A typical GOME orbit lasts about 100 min, half of which are spent on the night side of the earth. During this phase GOME carries out several sequences of dark current and LED

measurements (pixel-to-pixel gain). Various temperature sensors spread over the entire focal plane assembly monitor the in-orbit temperature variations. Once a month, the internal calibration lamp is switched on over an entire orbit. During this sequence a series of lamp measurements with and without the solar diffuser permits the investigation of long term degradation of the diffuser and an update in the wavelength calibration of the diode arrays, respectively.

## **6.2 EARTH PROBE TOMS**

TOMS is an optical sensor to measure the albedo of the earth's atmosphere at six narrow spectral bands. The total ozone content is interrelated with changes of solar radiation in the near ultraviolet wavelengths so that the spatial distribution of the total ozone can be inferred by observing several near UV bands. In addition, the TOMS observation data can be used to make quantitative estimates of sulphur dioxide amounts in the near UV band. The Field of View (FOV) of TOMS is 3 x 3 degrees (swath width: 42 x 42 km) and its scanning angle is +/- 55.5 degrees (approx. 2,800 km of the ground surface) across the track. This wide swath width can cover the entire earth surface in a day (NASA Facts Online, NASA Goddard Space Flight Centre).

The primary objective of TOMS is to collect data of the global ozone content and sulphur dioxide continuously. Combined with monitoring of ozone depletion above the south pole, which has been recently addressed as one of immediate environmental issues, and changes of ozone content after implementation of the Chlorofluorocarbons (CFC) Protocol, the data can be used for the quantitative analysis of factors related to the ozone issues and the potential effects of volcanic eruptions on climatic changes.

TOMS aboard Nimbus-7 and Meteor-3 provided global measurements of total column ozone on a daily basis and together provide a complete data set of daily ozone from November 1978 - December 1994. After an eighteen month period when the program had no on-orbit capability, ADEOS TOMS was launched on August 17, 1996 and provided data until June 29, 1997. Earth Probe TOMS was launched on July 2, 1996 to provide supplemental measurements, but was boosted to a higher orbit to replace the failed ADEOS. Earth Probe continues to provide near real-time data.

The EP-TOMS instrument is a second-generation backscatter ultraviolet ozone sounder. TOMS can measure "total column ozone"—the total amount of ozone in a "column" of air from the Earth's surface to the top of the atmosphere—under all daytime observing and geophysical conditions. TOMS observations cover the near ultraviolet region of the electromagnetic spectrum, where sunlight is absorbed only partially by ozone.

TOMS makes 35 measurements every 8 seconds, each covering 50 to 200 kilometres wide on the ground, strung along a line perpendicular to the motion of the satellite. Almost 200,000 daily measurements cover every single spot on the Earth except areas near one of the poles, where the Sun remains close to or below the horizon during the entire 24-hour period.

In addition to various "housekeeping" sensors to monitor the well-being of the instrument, TOMS uses several in-flight calibration modes to assess system performance. The solar irradiance is measured using a diffuser plate to reflect sunlight into the instrument. Actually, three diffuser plates are installed, which are used at different frequency. Comparisons of the signals of these diffusers allow the determination of degradation rates of the diffusers (McPeters et al., 1998).

In the next two sections EP-TOMS version 7 Archive Overpass ozone data (53.32 °N, 9.59 °E) and GOMEDOAS (DOAS algorithm ozone column determined from GOME spectra) with values within 500 km around (53.00 N, 9.00 E) were used.

### **6.3 DOAS BREMEN**

The ground based instrument was set up at the roof top (fifth floor) of the IUP-Bremen (53 °N, 9 °E). Absorption spectra in the UV / visible are detected in zenith sky viewing geometry. The experimental setup consists of a f/500 Czerny Turner spectrograph with 1024 pixel Reticon diode-array detector. The entrance slit of the spectrometer is connected to a zenith pointing telescope via a depolarizing quartz-fibre bundle. The spectral range of the instrument is 320 to 500 nm with a FWHM of 1 nm (Richter et al., 1995). A second instrument, taking care of the visible region, with a similar configuration but a wavelength range of 400 to 700 nm and a resolution of 1.4 nm FWHM was operated in parallel and used to deduce the vertical columns of O<sub>3</sub> and NO<sub>2</sub>. From these the species O<sub>3</sub>, NO<sub>2</sub>, and BrO are retrieved routinely (Richter et al., 1999). The measurements are part of the GOME validation campaign, the SCIAMACHY project and also part of the BREDOM concept.

The trace gas retrieval of O<sub>3</sub> and NO<sub>2</sub> is achieved using the DOAS technique (as already discussed in chapter three). For this study, the spectral window from 332 to 339 nm has been used, the spectra of O<sub>3</sub>, NO<sub>2</sub>, O<sub>4</sub> and a reference Ring spectrum being fitted (Richter, 1997). In this particular study a unique Optical Density Index (ODI) was used as the cross-section for the O<sub>3</sub> fit. This has the airmass factors (AMF) already included given a flexibility to compute the vertical columns of O<sub>3</sub> from the slant columns derived from the IUP DOAS algorithm of trace gases.

The AMF describes the effective length of the light path through the atmosphere and is derived from radiative transfer calculations, GOMETRAN (Rozanov et al., 1997, 2001). The value of the AMF depends on the viewing geometry and the solar zenith angle, but also on surface albedo, vertical gas profile, clouds and atmospheric aerosol.

## **6.4 Results and Discussion**

The four panels shown in Figure 6.1 indicate the vertical column of Ozone measured over Bremen using the instruments described in the previous three sections above. Since the overpass time for TOMS and GOME differ slightly, the GOME data set was shifted by  $-0.5$  days to match the time axis of TOMS and the ground-based data. The upper left panel shows the comparison of the total column between the satellites and the ground based DOAS Bremen (hereafter referred to as HB). There is a great variability shown during the beginning of the year. EP-TOMS registered both the minimum and maximum values (about 250 and 500 Dobson units by the close of February). The GOME data had a gap at the beginning of spring. Nevertheless, the three instruments show a good correlation during the summer period whilst the deviation is again pronounced by December. In order to carefully assess the performance of the instruments each satellite instrument was compared with HB in which case the average and root-mean-square (RMS) values were found for the differences.

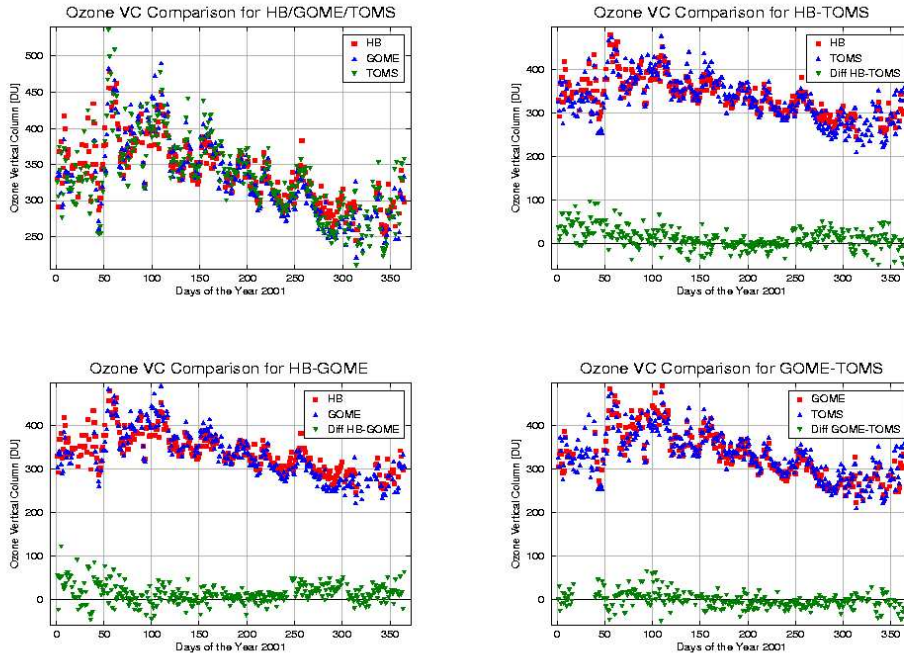


**Figure 6.1** 2001 Ozone vertical columns over Bremen measurements from the ground, DOAS Bremen (HB), and space, GOME and EP-TOMS satellites

There is a strong anti-correlation between TOMS and DOAS Bremen at the beginning and towards end of the year. This is depicted in the difference between the two spectra shown in green on the upper right panel. It showed quite a high negative difference. On the other hand, the difference between GOME and DOAS Bremen shows a fair matching with the best trend shown during the summer months. More importantly there is a positive difference in November-December as against the large negative in the case of TOMS. Notably, all instruments show good correlation in July-September.

Quantitatively the mean and RMS values for the difference between HB and GOME was found to be 3.6 DU and 21.7DU respectively. For the difference between HB and TOMS, 2.3 DU and 22.9 DU respectively were found. Also, the July to September mean and RMS values were found to be 8.9 DU and 13.1 DU and  $-0.8$  DU and 12.7 DU, for HB-GOME and HB-TOMS respectively. This gives an overall impression that summer total ozone columns as measured by the three instruments are comparably similar.

Indications are that the EP-TOMS had some calibration problems during the year under review and this could be attributed to the poor performance (the lowest and highest values measured over the period) against the other instruments (NASA Facts Online). DOAS Bremen also registered some lapses in its data quality due to shutter problems earlier during the year but this was rectified in time to ensure the quality of the data. Nonetheless, from the absolute values computed, the three instruments could be assessed as measuring nearly comparable values in 2001.

In general, measurements with satellite instruments compared with ground-based instruments have some discrepancies. The reference spectrum of the satellite measurements usually does not contain an absorption signal of the absorber under investigation. This is mainly because the detected sunlight for the reference spectrum comes directly from the sun and has not travelled through the earth's atmosphere. On the other hand, the reference spectrum of ground-based measurements contains an absorption signal of the investigated absorber ( $O_3$ ). Again, the use of space based instruments (like GOME) yield important information about the global distribution of atmospheric constituents, whereas the ground based measurements yield important information on the diurnal variation of the species, and are therefore useful to test our current understanding of the atmospheric chemistry.

On the whole, the large variability noticed in the winter-spring total columns of ozone may be linked to the relatively large horizontal size of the satellite pixel (in the case of GOME, 40 x 320 km). The light arriving at the detector has not travelled the same path through the atmosphere and this could be accountable for the difference in sensitivity.

## **6.5 MAX-DOAS Measurement over Bremen and Nairobi**

With the implementation of the multiple viewing geometries of the standard DOAS instrument, selected data from the Bremen and Nairobi (first tropical station) were analysed for the detection of ozone and NO<sub>2</sub> slant columns.

### **6.5.1 First Off-Axis Measurement in the Tropics (Nairobi)**

The successful installation of the first ever to be operated DOAS instrument in a tropical site like Nairobi is the first step in filling the data gap for centuries now. Exciting measurements from the Off-axis geometry innovation will reveal the photochemical smog situation over the city of Nairobi from the human activities and the automobile engines (tropospheric NO<sub>x</sub> and volatile organic compounds). The results shown below (Figure 6.2) give the NO<sub>2</sub> and O<sub>3</sub> slant columns from all the viewing geometries possible.

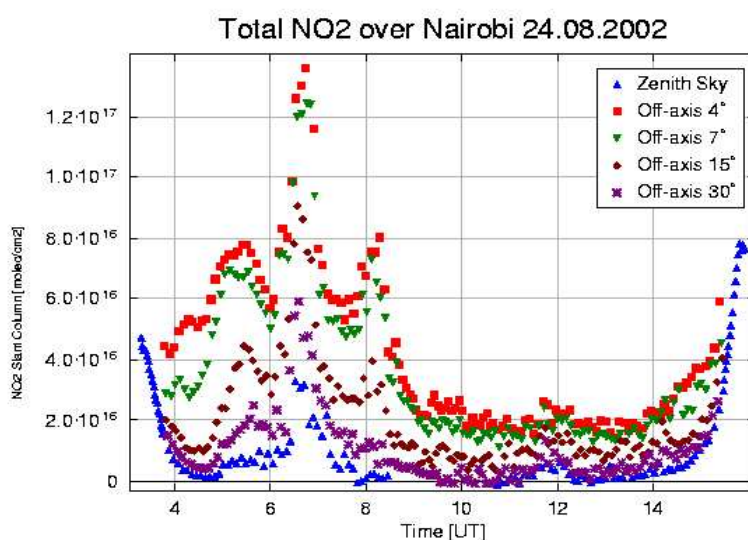
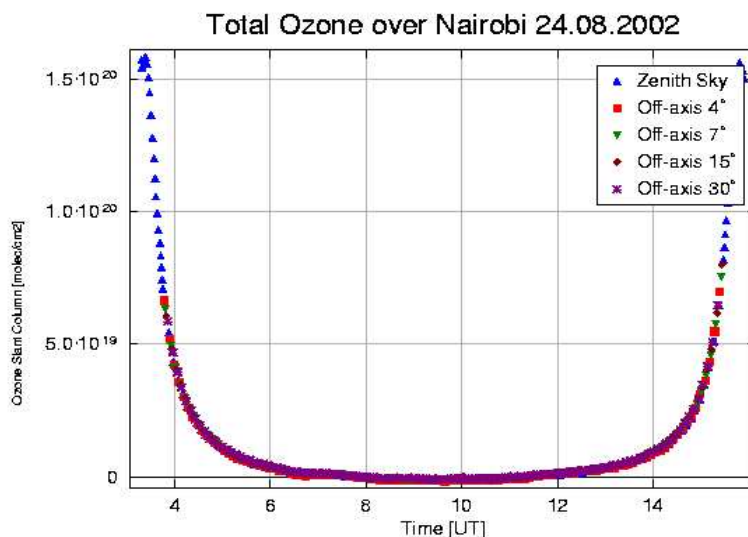


**Figure 6.2** Ozone and NO<sub>2</sub> measured over Nairobi on 24.08.2002

The top panel of Figure 6.2 shows the retrieved slant column of O<sub>3</sub> whilst the lower panel shows the NO<sub>2</sub> for all the viewing geometries implemented in the MAX-DOAS. The DOAS algorithm was used in the analysis with zenith sky (O<sub>3</sub> and NO<sub>2</sub>) measurements at noon as background. The O<sub>3</sub> and NO<sub>2</sub> absorption cross-sections used were those measured with the GOME satellite instrument (Burrows et al., 1998, 1999), O<sub>4</sub> from Greenblatt et al., (1990) and BrO from Wahner et al., (1988). Also, the warm and cold O<sub>3</sub> (temperatures of 221 and 241 K)

and NO<sub>2</sub> (221 and 293 K) were fitted using the wavelength window of 344.7 to 365 nm. The total slant columns were then computed by way of adding the warm and cold columns.

From the Figure above, all the viewing directions registered nearly the same total slant column of O<sub>3</sub> during the whole day. This indicates the detection of stratospheric O<sub>3</sub> on the 24th August. In contrast, the NO<sub>2</sub> columns show a clear distinction between the tropospheric and stratospheric contributions (depicting the power of the different lines of sights). The data gap in the zenith sky noon measurement for the NO<sub>2</sub> is the result of preventing direct sunlight from entering the telescope since it severely degrades the data quality. At noon the off-axis is automatically selected in which case the sun does not enter the field of view of the telescope. The highest NO<sub>2</sub> production was measured during the morning getting to noon with almost  $1.4 \times 10^{17}$  molec/cm<sup>2</sup> at around 10.00 am (local time). The value is measured with the lowest line of sight implemented at the station (4 ° above the horizon). At least all the off-axis viewing geometries indicated quite high values within the same time period (representative of tropospheric pollution). It was noticed that the weather was clear during the first half of the day and then deteriorates to cloudy situation in the afternoon.

In urban areas, under stable meteorological conditions (with almost no vertical exchanges and little ventilation), nitric oxide and volatile organic compounds and releases from cars accumulate in the boundary layer. With the clear weather situation the NO<sub>2</sub> builds up during the morning rush hour from the cars in the city. Thus the pollution scenario intended for investigation at the station (from human activities and vehicular discharges) is being sensed on this particular day in question.

## 6.2.1 Bremen Off – Axis Measurement

A similar analysis was performed with the two-day (27/7 and 01/8 2002) data from Bremen. Here the fitting window was changed slightly to 336.5 to 357 nm and O<sub>4</sub> and warm NO<sub>2</sub> were not fitted. The result is as shown in Figure 6.3 below.

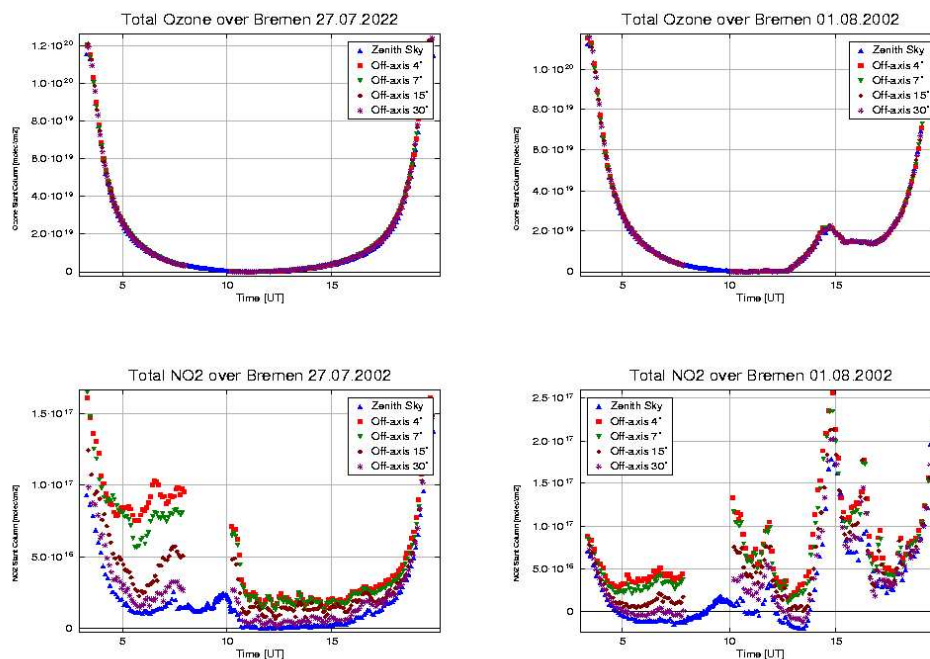


**Figure 6.3** Ozone and NO<sub>2</sub> slant columns over Bremen for July 27 and August 1, 2002

The different lines of sights show quite clearly different columns of NO<sub>2</sub> for the two different days whilst the O<sub>3</sub> total slant columns show similar magnitude for all the directions. It could be said that, as in the case of Nairobi, only stratospheric O<sub>3</sub> dominates the measurements on the different days. The August 1<sup>st</sup> O<sub>3</sub> value goes up around 17 hours local time to about  $2.0 \times 10^{19}$  molec/cm<sup>2</sup>.

For NO<sub>2</sub> the July 27<sup>th</sup> measurements show some high values in the morning for the off-axis lines of sight, which are well distinguished from the zenith sky measurements, clear weather situation. This trend changed getting to the evening and much closer values were measured

for both off-axis and zenith lines of sight. That is, columns in the troposphere and stratosphere are identified. The consistent gap in the off-axis directions is due to the exclusion of the  $-72$  and  $-32^\circ$  solar azimuth angles from the measurements to ensure that no direct sunlight (straylight) enter the field of view of the telescope (as explained for the zenith sky geometry in the previous section for solar zenith angle of  $20^\circ$  at noon).

The August 1<sup>st</sup> situation varies quite dramatically for all viewing directions by the evening. Zenith and the off-axis  $4^\circ$  registered  $\text{NO}_2$  values around  $2.6 \times 10^{17}$  molec/cm<sup>2</sup>. It was noted that around the same period the  $\text{O}_3$  values for all the lines of sight were also strongly enhanced. This was a clear indication for a tropospheric pollution scenario. There was thunderstorm in the afternoon and as a result abundant  $\text{NO}_2$  and  $\text{O}_3$  were produced by lightning, the sensitivity of the measurements further being enhanced by multiple scattering. The presence of clouds can limit the extent of all viewing paths, as long as the bottom of the clouds is above the altitude of the spectrograph. Here the cloud was huge and also very low to the extent that no matter in which direction measurements were made, the signal was always dominated by the clouds. Thus the zenith and off-axis geometries measured similar high values. This also accounted for the equal  $\text{O}_3$  value measured on the same day in the afternoon for the different viewing directions.

## 7 Summary and Conclusion

During the course of this study, a new generation MAX-DOAS instrument was successfully calibrated and installed in Nairobi. The instrumental setup and the main new features implemented in the standard zenith sky DOAS were substantially discussed. The Andor CCD camera and the Oriel LOT spectrograph was tested for dark current, linearity, polarisation dependency and the instrument slit function.

The dark current measurement was performed on two CCD chips, 2722 and 2720. Large offset was found in the case of CCD 2722 and this was attributable to the time taken for cooling and running the CCD and possibly the instrument settings. In Figure 5.4 it was shown that the 2720 and 2722 have dark current of 0.003 count / pixel / sec and 0.03 count / pixel / sec respectively. Meaningful operational temperature levels for the CCD were determined to be around  $-40$  and  $-45$  °C. It was found that the dark signal increases with increasing temperature. The limits for the useful range of the detector signal readout were also established with a revelation of defects in the CCD. A stabilised white light was used to scan through the entire CCD covering all the possible wavelengths (the left, middle and right part of the CCD). Figure 5.5 showed the non-uniformity of the CCD. Some portions show saturation as low as 16 kilocounts and 26 kilocounts and then as high as above 35 kilocounts. These varying deviations from linearity (which was poorer than 1 %) and saturation levels do not guarantee good measurements and so the CCD was recommended for further testing by the manufacturers.

The scattered light received by the telescope is always polarised by the air molecules from the atmosphere, especially Rayleigh scattering. To ensure that the spectrometer is measuring the required absorbers over the location, the polarisation dependency test was effectively carried

out. The results show that the quartz-fibre bundle being used is helping in depolarising the light. The instrument slit function, needed for the convolution of the cross-sections for the spectrometer was detected to be of a poor standing for the tested instrument. Figure 5.6 shows the nonuniformity in the shape of the spectrum measured. This does not guarantee an optimal convolution of the cross-section. Nevertheless, the band pass did not show any appreciable change and as a result the spectrometer was subjected to further adjustment before incorporating it into the final setup.

A validation exercise was performed using 2001 data set from ground based and satellite instruments. The zenith sky DOAS instrument, which has been in operation since 1993, was used in validating the total ozone columns over Bremen measured with the EP-TOMS and GOME satellite instruments. The results indicated a big variability in the ozone columns measured during the beginning of the year 2001 with TOMS delivering both the lowest and highest values. Good correlation was then noticed as the year progresses and the best period of close matching among the instruments was recorded in summer 2001 (July to September). The mean and root-mean-square values computed for the difference between the satellite instruments and the ground-based DOAS showed that all three instruments measured comparable total O<sub>3</sub> columns during summer. Mean and RMS values of 8.9 DU, 13.1 DU and -8.3 DU, 12.7 DU for GOME and TOMS differenced against DOAS HB respectively from July to September (summer months) was measured. The nearly same RMS (scatter) values indicated a strong correlation among these instruments notwithstanding the discrepancies between a satellite and ground based instruments (see Figure 6.1).

First measurements from the MAX-DOAS setup in Bremen and Nairobi, implemented for the first time in the midlatitudes and tropics showed a distinctive feature for the off-axis lines of sight. The few selected days in July and August 2002 showed morning twilight NO<sub>2</sub> high

slant column in the boundary layer over Nairobi on August 24<sup>th</sup>. This result is quite indicative of the early morning (rush hour) heavy pollution from automobiles in the city. Evening twilight high NO<sub>2</sub> and O<sub>3</sub> slant columns were measured over Bremen on August 1<sup>st</sup>. This was attributable to the thunderstorm and the pollution situation. The thick and low clouds observed in the afternoon resulted in similar measurements from all the viewing directions. This brings into focus the work by Erle et al., 1995 that in evaluating the amount of a tropospheric species using total column measurements, consideration of path enhancement due to tropospheric clouds must be considered. The potential for an apparent enhancement of a tropospheric absorber exists due to an increase in the tropospheric portion of the light path created by Mie scattering within the clouds. The presence of such an enhancement would affect all absorbers located in the troposphere.

The high NO<sub>2</sub> slant column measured during the first half of July 27<sup>th</sup> for the off-axis direction is indicative of tropospheric pollution (see Figure 6.3). These qualitative results are clear indications of the fact that the introduction of the different lines of sight near the horizon as additional light sources to the well-known UV / vis instruments is a real advantage. That is, the MAX-DOAS setup technique does not only derive the column amounts of different trace gases but also gives some information about the location of the absorbers. The information so gotten from the measurements will necessitate further investigation about the consistency of trace column amounts derived from different platforms (see earlier work done by Wittrock et al., 2002).

Further work (which is already ongoing in the DOAS group) has to be carried out in a more quantitative manner to fully explore the potential of the MAX-DOAS technique. Interpretation of the results using the full-spherical radiative transfer model (for instance, SCIATRAN) requires urgent attention. Assumption of only cloud-free scenarios in the

airmass factor calculation has to be extended and studied to include the cloudy sky, which is a real life occurrence.

## References

- A user's Guide to Andor CCDs, PCI Edition, Version **2B**, Andor Technology Limited 1999.
- Bassford, M. R., C. A. McLinden, K. Strong, Zenith-sky observations of stratospheric gases: the sensitivity of air mass factors to geophysical parameters and the influence of tropospheric clouds, *JQSRT* **68**, 657-677, 2001.
- Borrell, Peter, An essay written for the Encyclopedia of Ecology and Environmental Management, Ed. Peter Calow, Blackwell Science, Oxford, 1998.
- Bovensmann, H., J. P. Burrows, M. Buchwitz, J. Frerick, S. Noël, V. V. Rozanov, K. V. Chance, and A. H. P. Goede *SCIAMACHY - Mission objectives and measurement modes*, *J. Atmos. Sci.*, **56**(2), pp. 127-150, 1999.
- Burrows, J. P., M. Weber, V. Rozanov, A. Ladstätter-Weissenmayer, and R. Richter, Global Ozone Monitoring Experiment (GOME): mission concept and first scientific results, *J. Atmos Sc.* **56**, 127-150, 1999.
- Burrows, J. P., A. Richter, A. Dehn, B. Deters, S. Himmelmann, S. Voigt, and J. Orphal, Atmospheric Remote-Sensing Reference Data from GOME: Part 2. Temperature Dependent Absorption Cross Sections of O<sub>3</sub> in the 231 –794 nm Range, *J. Quant. Spectrosc. Radiat. Transfer*, **61**, 509-517, 1999c.
- Burrows, J. P., A. Richter, A. Dehn, B. Deters, S. Himmelmann, S. Voigt, and J. Orphal, Atmospheric Remote-Sensing Reference Data from GOME: Part 2. Temperature Dependent Absorption Cross Sections of NO<sub>2</sub> in the 231 –794 nm Range, *J. Quant. Spectrosc. Radiat. Transfer*, **60**, 1025-1031, 1998d.
- Chance, K., P. I. Palmer, R. J. D. Spun, R. V. Martin, T. P. Kurosu, and D. J. Jacob, Satellite observations of formaldehyde over North America from GOME, *Geophys. Res. Lett.*, **27**,3461-3464, 2001.
- Chapman, S., A theory of upper atmospheric ozone, *Mem. R. Metoerol. Soc.*, **3**, 103-125, 1930.
- Czerny, M. and A.F. Turner, Über den Astigmatismus bei Spiegelspektrometern, *Z. Phys.*, **61**, 792, 1930.
- Dobson, G. M. B., Forty years' research on atmospheric ozone: a history, *Applied Optics* **7**, 387, 1968.
- Eisinger, M., and J. P. Burrows, Tropospheric Sulphur Dioxide observed by the ERS-2 GOME instrument, *Geophys. Res. Lett.*, **25**, 4177-4180, 1998.
- Erle, F., K. Pfeilsticker, and U. Platt, On the influence of tropospheric clouds on the zenith-scattered-light measurements of stratospheric species, *Geophys. Res. Lett.*, **22**, 2725-2728, 1995.

Fishman, J., and P. Crutzen, The origin of ozone in the troposphere, *Nature*, **274**, 855-858, 1978.

GOMEMANUAL, 1995 GOME Users Manual, ESA Special Publication 1182, ESA/ESTEC, Noordwijk, The Netherlands.

Hoeningner, G., Halogen Oxide Studies in the Boundary Layer by Multi Axis Differential Optical Absorption Spectroscopy and Active Longpath-DOAS, *Ph.D Thesis, University of Heidleberg, Germany, 2002*.

Junge, C.E., Global ozone budget and exchange between stratosphere and troposphere, *Tellus*, **14**, 363-377, 1963.

Kurylo, M. J., Network for the Detection of Stratospheric Change (NDSC), *J. Atmos. Chem.*, **1491**, 168-174, 1991.

Ladstätter-Weißmayer, A., J. P. Burrows, P. Crutzen, and A. Richter, GOME: Biomass burning and its influence on the troposphere, in *European Symposium on Atmospheric Measurements from Space, ESA WPP-161, Vol 1*, pp. 369-374, 1999.

Lamarque, J. F., G. P. Brasseur, P. G. Hess, and J. F. Müller, Three-Dimensional study of the relative contributions of the different nitrogen sources in the troposphere, *J. Geophys. Res.*, **101**, 22955-22968, 1996.

Leue, T. W. C., K. Pfeilsticker, U. Platt, Monitoring of the stratospheric chlorine activation by GOME OClO measurements in Austral and Boreal winters 1995 through 1999, *J. Geophys. Res.*, **106**, 4971-4986.

McElroy, C. T., C. A. McLinden, J. C. McConnell, Evidence of bromine monoxide in the free troposphere during the Arctic polar sunrise. *Nature* **397**, 338-341, 1999.

McPeters, R. D., J. A. Kaye, J. R. Herman, P. K. Bhartia and A. J. Krueger, 'New TOMS Instrument Measures Ozone and Aerosols,' *EOS (Trans. AGU)*, **79**, 57,63, 1998.

Miller, H. L., A. Weaver, R. W. Sanders, K. Arpag, and S. Solomon, Measurements of Arctic Sunrise Surface Ozone Depletion Events at Kangerlussuaq, Greenland, *Tellus*, **49B**, 496-509, 1997.

Mount, G.H., R.W. Sanders, A. L., Schemeltekopf, and S. Solomon, Visible spectroscopy at Mc Murdo Station, Antarctica, 1., Overview and daily variations of NO<sub>2</sub> and O<sub>3</sub>, Austral spring, 1986, *J. Geophys Res.*, **92**, 8320, 1987.

Perliski, L. M. and Solomon, S., On the evaluation of Air Mass Factors for Atmospheric Near-Ultraviolet and Visible Absorption Spectroscopy, *JGR*, **98**, 10,363, 1993.

Plane, J.M.C., and N. Smith, 'Atmospheric Monitoring by Differential Optical Absorption Spectroscopy,' in *Spectroscopy in Environmental Science* (R.J.H. Clark and R.E. Hester, Eds.), 223-262, Wiley, New York, 1995.

Platt, U., 'Differential Optical Absorption Spectroscopy (DOAS),' in *Air Monitoring by Spectroscopy Techniques* (M.W. Sigrist, Ed.), Chemical Analysis Series **127**, 27-84, Wiley, New York, 1994.

Richter, A. and J.P. Burrows, Retrieval of Tropospheric NO<sub>2</sub> from GOME Measurements , *Adv. Space Res.*,**29(11)**, 1673-1683, 2002.

Richter, A., AMAX\_OMA Manual, version 1.8 (Internal Use only).

Richter, A., F. Wittrock, M. Eisinger, and J. P. Burrows, GOME observations of tropospheric BrO in Northern Hemispheric spring and summer 1997, *Geophys. Res. Lett.*, **25**, 2683-2686, 1998.

Richter, A. et al., Ground based UV / vis measurements of O<sub>2</sub>, NO<sub>2</sub>, BrO and OCIO over Bremen (53 °N), *Proc. Of the 18<sup>th</sup> Ozone Symposium in in L'Aquila*, 1997.

Richter, A., Ground based UV / vis measurements of stratospheric trace gases above Bremen (53 °N), *PhD Thesis, University of Bremen*, 1997 (in German).

Richter, A., M. Eisinger, A. Ladstätter-Weißenmayer, and J. P. Burrows, DOAS zenith-sky observations. 2. seasonal variation of BrO over Bremen (53 °N) 1994-95, *Journal of Atmospheric Chemistry*, **32**, 83-99, 1999.

Richter, A. et al., Ground based UV / vis measurements of O<sub>3</sub>, NO<sub>2</sub>, BrO, and OCIO over Bremen (53 °N), *Proc. 3<sup>rd</sup> Europ. Symp. On Stratospheric Ozone, Schliersee*, 1995.

Rozanov, V., D. Diebel, R. Spurr and J.P. Burrows, GOMETRAN: A radiative transfer model for the satellite project GOME-the plane parallel version, *J.Geophys. Res.*, **102**, 16683-16695, 1997.

Rozanov, A., V. Rozanov, and J. P. Burrows, A numerical radiative transfer model for a spherical planetary atmosphere: Combined differential-integral approach involving the Picard iterative approximation, *Journal of Quantitative Spectroscopy and Radiative Transfer*,**69**, 4135-4142, 2001.

Sanders, R. W., S. Solomon, J. P. Smith, L. Perliski, H. L. Millr, G. H. Mount, J. G. Keys, and A. L. Schmeltekopf, Visible and Near-Ultraviolet Spectroscopy at McMurdo Station Antarctica, 9. Observations of OCIO from April to October 1991, *J. Geophys. Res.*, **98(D4)**, 7219-7228, 1993.

Sarkissian, A., H. K. Roscoe, D. J. Fish, Ozone measurements by zenith-sky spectrometers: an evaluation of errors in air-mass factors calculated by radiative transfer models, *JQSRT* **54**, 471-480, 1995.

Solomon, S., Stratospheric Ozone Depletion: A review of concepts and history, *Review of Geophysics*, **37**, 275-316, 1999.

System Performance, Andor Technology Limited, **Issue 1, Rev. 8**, 2001.

Thomas, W., E. Hegels, S. Slijkhuis, R. Spurr, and K. Chance, Detection of biomass burning combustion products in Southeast Asia from backscatter data taken by the GOME spectrometer, *Geophys. Res. Lett.*, **25**, 1317-1320, 1998.

Velders G. J. M., C. Granier, R. W. Portmann, K. Pfeilsticker, M. Wenig, T. Wagner, U. Platt, A. Richter, and J. P. Burrows, Global tropospheric NO<sub>2</sub> column distributions: Comparing 3-D model calculations with GOME measurements, *J. Geophys. Res.*, **106(D12)**, 12643-12660, 2001.

Wagner, T., and U. Platt, Satellite mapping of enhanced BrO concentrations in the troposphere, *Nature*, **395**, 486-490, 1998.

Wayne, R. P., *Chemistry of Atmospheres*, Oxford University Press, 1991.

Weber, M., J.P. Burrows and R.P. Cebula, GOME Solar UV/VIS Irradiance Measurements between 1995 and 1997 - First Results on Proxy Solar Activity Studies, *Solar Physics* **177**, 63-77, 1998.

Wittrock, F. H. Oetjen, A. Richter, A. Rozanov, and J. P. Burrows, MAX-DOAS measurements of atmospheric trace gases to be submitted to *Applied Optics*.

World Meteorological Organisation, *Scientific Assessment of Ozone Depletion*: 1994.

WMO, Geneva, Switzerland, 1994.

## **Acknowledgement**

I wish to express my profound gratitude to the chairman of the Postgraduate Programme in Environmental Physics (PEP) Prof. Dr. J. Bleck-Neuhaus for his strong sense of commitment to the welfare of students of the infant programme. The entire well-informed PEP-TEAM deserves a pat on their shoulders from me for their unrelenting efforts in attending to students' beck and call.

I am indebted to my Principal Supervisor, Prof. Dr. J. P. Burrows for gladly accepting me into his research group. I also thank him for his words of encouragement during the course of preparing this thesis. My Tutor, Dr. Andreas Richter deserves special thanks for his patience, love, concern and the great motivation given me since I joined the DOAS group for the preparation of my Master Thesis. Without his efforts and coaching this work would not have seen the dawn of the day. And I say more grease to your elbows and congratulations.

To the entire big crew of the DOAS group I say God richly bless you for your help. Dr. Astrid Löwe and Folkard Wittrock deserve a special mention here for their numerous suggestions and help. To the many other Lecturers and Scientists of the Institute of Environmental Physics I say thank you for your concern. Also, I say bravo to all my colleagues of the PEP programme. It is impressive to have come to know you from different parts of the world.

My sweetheart, Eternam I say without you life would have been very difficult for me. Thanks for your care and love. To all and sundry, I say Jehovah bless you.